PHILOSOPHICAL TRANSACTIONS OF THE ROYAL SOCIETY A MATHEMATICAL, PHYSICAL & ENGINEERING SCIENCES

Electrohydrodynamic Deformation and Burst of Liquid Drops

S. Torza, R. G. Cox and S. G. Mason

Phil. Trans. R. Soc. Lond. A 1971 **269**, 295-319
doi: 10.1098/rsta.1971.0032

ELECTROHYDRODYNAMIC DEFORMATION AND BURST OF LIQUID DROPS

By S. Torza, R. G. Cox and S. G. Mason
Pulp and Paper Research Institute of Canada, and
Department of Chemistry, McGill University, Montreal, Canada

(*Communicated by Sir Geoffrey Taylor, F.R.S.—Received* 20 *July* 1970)

[Plates 6 and 7]

CONTENTS

In 60 Hz electric fields, liquid drops suspended in a second immiscible liquid deformed into prolate spheroids oriented in the direction of the field in 22 drop/medium combinations studied experimentally. In steady fields, oblate or prolate spheroids were formed depending upon the dielectric constants and resistivities of the drop and medium. In systems yielding oblate spheroids, a critical frequency existed at which the drop remained spherical at all field strengths. Electrohydrodynamic streaming near the surface of the drop occurred as predicted by Taylor.

A theory, valid for both steady and alternating fields, was developed which predicts the conditions leading to oblate and prolate spheroids and which reduces to Taylor's equations for conducting dielectrics in steady fields and to the equations for perfect dielectrics in steady and alternating fields. The theory explains the general types of deformation and electrohydrodynamic flow which were observed and predicts several interesting new modes of behaviour. In most cases the measured deformations were greater than calculated from the theory; various explanations for this discrepancy are advanced, but no definite conclusions are reached.

At high field strengths the drops burst in two basically different ways which we have designated as electric and electrohydrodynamic burst, the first caused by electric stresses alone and the second by a combination of electric and hydrodynamic stresses.

Vol. 269. A. 1198. (Price £0.85; U.S. $2.20) 27 [Published 18 February 1971

List of symbols

a	$= \epsilon_0 \chi_1 K_2$
A; $\bar{A}$	complex quantity defined by equation (11); its complex conjugate
b; b_1, b_2	radius of the spherical drop; principal radii of curvature of the deformed drop surface
$C_{1n}^*, C_{2n}^*, C_{3n}^*, C_{4n}^*$	complex constants of integration characterizing V_1^* and V_2^*
C_5, C_6, C_7, C_8	constants of integration characterizing ψ
d_1', d_2'; d_1, d_2	axes of the deformed drop parallel and normal to E; steady values
D_ν'; D_ν, D_{T}	$= (d_1' - d_2')/(d_1' + d_2')$, total drop deformation at frequency ν; its steady and oscillatory components
E; $E_0, \bar{E}_0$	undisturbed oscillating electric field; its amplitude and root-mean-square value
$\boldsymbol{E}_j'$; $E_{jr}, E_{j\theta}$	complex electric field inside ($j = 1$) and outside ($j = 2$) the drop; its real, radial and transverse components at $r = b$
$(\bar{E}_0)_{\max}$	limiting value of the electric field calculated from equation (83)
$f_{r\nu}, f_{r\mathrm{T}}$	steady and oscillatory total normal stress at $r = b$
$F_{r\nu}'$; $F_{r\nu}, F_{r\mathrm{T}}$; F_r^*	radial component of the electric stress at $r = b$; steady and oscillatory components; complex quantity defined by equation (22a)
$F_{\theta\nu}'$; $F_{\theta\nu}, F_{\theta\mathrm{T}}$; F_θ^*	transverse component of the electric stress at $r = b$; steady and oscillatory components; complex quantity defined by equation (22b)
g_j; $g_{\min}$	functions defined by equations (84); least of these functions
$h^*, \bar{h}^*$; H^*	complex quantity defined by equation (60) and its complex conjugate; complex quantity defined by equation (59)
I	real quantity related to D_{T} and defined in equation (63b)
k	$= \omega b \mu_2 / \gamma$
K_1, K_2	dielectric constants of the drop and of the medium
m_ν; m_ν^*	parameter defined by equation (77); experimental value
$p_{rr}, p_{r\theta}$; p_{jrr}^{I}, $p_{jr\theta}^{\mathrm{I}}$; $p_{jrr}^{\mathrm{II}}, p_{jr\theta}^{\mathrm{II}}$	hydrodynamic stress components for an axisymmetric flow field in the radial and transverse directions; inside ($j = 1$) and outside ($j = 2$) the drop for the fluid flow generated by $F_{\theta\nu}'$; and for the fluid flow generated $F_{r\mathrm{T}}$
$P_n(\cos\theta)$	Legendre polynomial of order n
q	$= K_1/K_2$
Q_{S}	total electric charge flux per unit length of surface
r, θ	spherical polar coordinates
R	$= \chi_1/\chi_2$
S, S_1, S_2	functions defined by equations (81)
t	time
$\boldsymbol{u}_j$; $u_{2\theta}$; $\boldsymbol{u}_j^{\mathrm{I}}, \boldsymbol{u}_j^{\mathrm{II}}$; $u_{jr}^{\mathrm{I}}, u_{j\theta}^{\mathrm{I}}, u_{jr}^{\mathrm{II}}, u_{j\theta}^{\mathrm{II}}$	total velocity field inside ($j = 1$) and outside ($j = 2$) the drop; total external transverse component; components generated by $F_{\theta\nu}'$ and by $F_{r\mathrm{T}}$; radial and transverse components
U_ν^{I}; $U_{\mathrm{S}}^{\mathrm{I}}, U_{\mathrm{T}}^{\mathrm{I}}$; $U_{\mathrm{T}}^{\mathrm{II}}$	quantity defining $\boldsymbol{u}^{\mathrm{I}}$; its steady and oscillatory components; quantity defining $\boldsymbol{u}^{\mathrm{II}}$
V_j, V_j', V_j^*	electric potentials, complex time-dependent values and complex amplitude both inside ($j = 1$) and outside ($j = 2$) the drop

PHILOSOPHICAL TRANSACTIONS OF THE ROYAL SOCIETY A MATHEMATICAL, PHYSICAL & ENGINEERING SCIENCES

w_S, w_T	constants defining F'_{rv} and given by equations (21)
W_r, W_θ	radial and transverse components of a general axisymmetric flow field
$\alpha_\nu, \alpha_\nu^{I}, \alpha_\nu^{II}$	phase angles respectively defined in equations (15*b*), (36*d*), (36*e*) and (63*a*)
γ	interfacial tension
ϵ_0	permittivity of free space
$\lambda; \lambda_1, \lambda_2$	viscosity radio $= \mu_1/\mu_2$; functions of λ defined by equations (58)
$\mu; \mu_1, \mu_2$	viscosity; value for the drop and for the medium respectively
$\nu; \nu_c; \omega$	frequency of the field; critical value; angular frequency $= 2\pi\nu$
ρ	density of the liquid
$\sigma; \sigma', \sigma^*$	charge density on the drop surface; related complex quantities
$\Phi'_\nu; \Phi_\nu$	total discriminating function; steady value
$\chi_1, \chi_2; \chi_{12}$	resistivities of the drop and of the medium; surface resistivity
ψ	Stokes steam function
Re	symbol denoting the operation of taking the real part of the complex values

1. Introduction

When a fluid, containing an immiscible fluid drop, is subjected to an electric field, the drop deforms at low fields into a prolate or an oblate spheroid whose axis of rotation is in the field direction and usually bursts at high fields (Wilson & Taylor 1925; Buchner & Van Royen 1929; O'Konski & Gunther 1955; O'Konski & Harris 1957; Kao 1961; Schwarz 1962; Allan & Mason 1962; Garton & Krasucki 1964; Taylor 1964, 1966; Iribarne & Mason 1967).

When the medium is a perfect dielectric, deformation into a prolate spheroid and subsequent burst of the drop are readily explained by a straightforward theoretical analysis in which the normal electric stress at the interface is balanced by the capillary pressures generated by the changes in curvature of the drop surface (Nayyar & Murthy 1959; Allan & Mason 1962; Garton & Krasucki 1964); an identical result is obtained from energy equations (O'Konski & Thacker 1953; O'Konski & Gunther 1955; O'Konski & Harris 1957).

When an oblate spheroid is formed it has been noted that the medium is electrically conducting (Buchner & Van Royen 1929; Allan & Mason 1962). Taylor (1966) recognized that in this circumstance there is a transverse electric stress (absent when the medium is a perfect dielectric) at the interface which generates flow inside and outside the drop, and developed an electrohydrodynamic theory which takes into account the additional stresses associated with the flow. The theory predicts: (i) the formation of both oblate and prolate spheroids depending upon the ratios of the dielectric constants, the electric resistivities and viscosities of the two phases; and (ii) the existence of critical values of the ratios at which the drop remains spherical. Reasonably convincing qualitative evidence of the general validity of this theory, including the predicted patterns of flow, has been presented based on experiments conducted in zero frequency ($\nu = 0$) fields (Taylor 1964; Melcher & Taylor 1969).

Experiments at $\nu = 0$ are rendered difficult by electrophoretic migration of the drops when these acquire a small net electric charge. Since electrophoresis is eliminated when $\nu > 0$, we decided to repeat some of the earlier experiments of Allan & Mason (1962) using both $\nu = 0$ and $\nu = 60$ Hz fields. To our surprise prolate spheroids were always formed at $\nu = 60$ Hz. This suggested that in systems which formed oblate spheroids at $\nu = 0$ there should exist a critical frequency ν_c (which in these cases was less than 60 Hz) at which there is no deformation no

PHILOSOPHICAL TRANSACTIONS OF THE ROYAL SOCIETY A MATHEMATICAL, PHYSICAL & ENGINEERING SCIENCES

matter how high the field; this was confirmed in experiments in which ν was varied continuously. A number of other differences in modes of deformation and burst between $\nu = 0$ and $\nu = 60\,\mathrm{Hz}$ were observed which could not be explained by Taylor's theory which, strictly speaking, applies only at $\nu = 0$.

After completing the experiments, we developed a generalized electrohydrodynamic theory for alternating fields which reduces to (i) Taylor's (1966) theory at $\nu = 0$ and (ii) Allan & Mason's (1962) theory when the phases are perfect dielectrics and which predicts the existence of ν_c under certain conditions. Following a line of reasoning similar to that of Taylor (1966) developed for $\nu = 0$, we assume that, in the general case, both drop and medium are leaky dielectrics each behaving as a perfect dielectric in parallel with an ohmic resistor. We then calculate the oscillating potentials inside and outside the drop, which we assume is nearly spherical and in turn the electric stress at the interface, expressing the normal and transverse components as sums of a steady and an oscillating part. The transverse and the oscillating normal electric stress generate flow with associated hydrodynamic stresses at the interface which are calculated from the velocity field made to satisfy the Navier–Stokes equation, inertial effects being neglected. The total normal stress, the sum of the electric and hydrodynamic components, is then used to calculate the drop deformation as the sum of a steady and oscillating part.

The theory, which explains most the of experimental findings described later, will now be presented in detail.

2. Theoretical part

2.1. *Electric stress at the drop surface*

We consider a drop of radius b which carries no net electric charge and is suspended in a neutrally buoyant condition in an immiscible fluid subject to a uniform electric field whose strength E, far from the drop, varies with time t according to

$$E = E_0 \cos \omega t, \tag{1}$$

where $\omega = 2\pi\nu$ is the angular field frequency of the field, E_0 is the peak value of the field when $\nu > 0$ and the steady value when $\nu = 0$. We assume that the dielectric constants K_1 and K_2 and the ohmic resistivities χ_1 and χ_2 of the drop and medium respectively are independent of ν.

Taking the centre of the drop as the origin of the spherical polar coordinates r, θ (figure 1*a*), in the absence of space charge the electric potentials inside (V_1) and outside (V_2) the drop both satisfy the Laplace equation

$$\nabla^2 V_j = 0 \quad (j = 1, 2), \tag{2}$$

with the following boundary conditions: (i) the electric potential tends to $(-Er\cos\theta)$ as $r \to \infty$ and is bounded at the drop centre; (ii) the difference between the electric displacements at the interface is equal to the surface charge density σ; (iii) $V_1 = V_2$ at $r = b$ and (iv) the rate of increase of σ is equal to the net flow of charge into the interface, transport of charge along the interface being neglected. The validity of the last assumption, which was made also by Taylor (1966) and Melcher & Taylor (1969), will be examined later. Finally the drop is assumed to remain nearly spherical so that the present theory gives a first order approximation to the deformation.

To simplify the calculations we introduce the complex electric potentials V_1' and V_2' inside and outside the drop such that their real parts are respectively V_1 and V_2 and both their real and imaginary parts separately satisfy equation (2). Writing

$$V_1' = V_1^* \, \mathrm{e}^{\mathrm{i}\omega t} \quad \text{and} \quad V_2' = V_2^* \, \mathrm{e}^{\mathrm{i}\omega t}, \tag{3}$$

the time-independent complex quantities V_1^* and V_2^* are defined by the following relations expressing in complex form the boundary conditions mentioned above:

$$V_2^* \to -E_0 r\cos\theta \quad \text{as} \quad r\to\infty; \tag{4a}$$

$$V_1^* = V_2^* \quad \text{at} \quad r=b; \tag{4b}$$

$$\epsilon_0 K_2 \frac{\partial V_2^*}{\partial r} - \epsilon_0 K_1 \frac{\partial V_1^*}{\partial r} = -\sigma^* \quad \text{at} \quad r=b; \tag{4c}$$

$$\frac{1}{\chi_2}\frac{\partial V_2^*}{\partial r} - \frac{1}{\chi_1}\frac{\partial V_1^*}{\partial r} = \mathrm{i}\omega\sigma^* \quad \text{at} \quad r=b; \tag{4d}$$

$$V_1^* \quad \text{bounded} \quad \text{at} \quad r=0, \tag{4e}$$

where σ^* is defined by

$$\sigma' = \sigma^* \mathrm{e}^{\mathrm{i}\omega t}, \tag{5}$$

the real part of the complex charge density σ' being equal to the charge density σ on the drop surface. The permittivity of free space $\epsilon_0 = 8.84\times10^{-12}\,\mathrm{m^{-2}\,s^2}$ is required in the m.k.s. system (SI) of units which we employ in the theory.

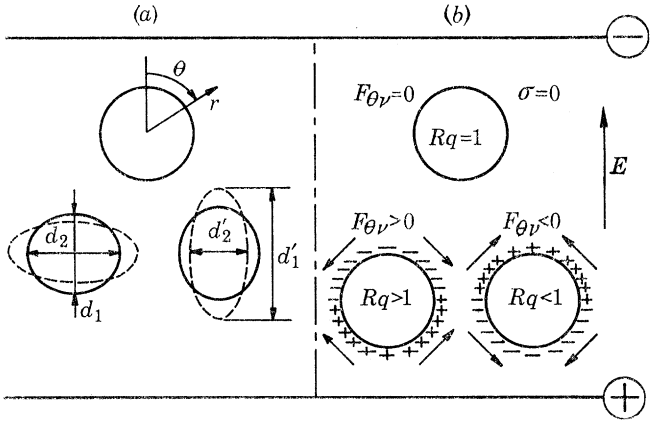

$$D_\nu' = \frac{d_1'-d_2'}{d_1'+d_2'} \qquad D_\nu = \frac{d_1-d_2}{d_1+d_2}$$

FIGURE 1. (*a*) Polar coordinates (r,θ) in an electric field $\boldsymbol{E} = -\nabla V$ directed toward decreasing potentials V. The steady (D_ν) and total (D_ν') deformation parameters of the drop are defined by the diameters d_1, d_2 and d_1', d_2' respectively. Steady oblate $(D_\nu < 0)$ and prolate $(D_\nu > 0)$ deformed drops are shown by the continuous lines respectively from left to right of the figure, the dotted lines indicating a transient shape during the oscillation about the steady value.

(*b*) Schematic representation of the instantaneous charge distribution and of the direction of $F_{\theta\nu}$ at the interface given by equations (15*a*) and (20*b*) for various values of the product (Rq). When $Rq > 1$ the hemisphere facing the negative electrode becomes negatively charged, $F_{\theta\nu}(>0)$ inducing a pole-to-equator flow; the reverse occurs when $Rq < 1$, $F_{\theta\nu}(<0)$ inducing an equator-to-pole flow. When $Rq = 1$, $\sigma = 0$, $F_{\theta\nu} = 0$ and there is no flow. For a complete description of the flow pattern see figure 5.

Eliminating σ^* from equations (4*c*) and (4*d*) yields

$$\left(\frac{1}{\chi_2} + \mathrm{i}\omega\epsilon_0 K_2\right)\frac{\partial V_2^*}{\partial r} = \left(\frac{1}{\chi_1} + \mathrm{i}\omega\epsilon_0 K_1\right)\frac{\partial V_1^*}{\partial r}. \tag{6}$$

Since V_1^* and V_2^* satisfy the Laplace equation, they may be written as (Smythe 1959):

$$V_1^* = \sum_{n=0}^{\infty} (C_{1n}^* r^n + C_{2n}^* r^{-n-1}) P_n(\cos\theta); \tag{7a}$$

$$V_2^* = \sum_{n=0}^{\infty} (C_{3n}^* r^n + C_{4n}^* r^{-n-1}) P_n(\cos\theta), \tag{7b}$$

where C^*_{1n}, C^*_{2n}, C^*_{3n} and C^*_{4n} are time-independent complex quantities and $P_n(\cos\theta)$ is the Legendre polynomial of order n.

From the boundary conditions given by equations (4*a*) and (4*e*) it follows that

$$C^*_{2n} = 0 \text{ for all } n; \tag{8a}$$

$$C^*_{3n} = 0 \text{ for } n \neq 1 \text{ and } C^*_{31} = -E_0 \cos\theta. \tag{8b}$$

As a solution we try:

$$V^*_1 = C^*_{11}\, r\cos\theta; \tag{9a}$$

$$V^*_2 = (-E_0 r + C^*_{41} r^{-2})\cos\theta. \tag{9b}$$

Substituting equations (9) into the remaining boundary conditions given by equations (4*b*) and (6), we obtain

$$C^*_{11} = -3E_0 A; \quad C^*_{41} b^{-3} = -(3A-1)E_0, \tag{10}$$

where

$$A = \frac{R + \mathrm{i}a\omega}{(2R+1) + \mathrm{i}a\omega(q+2)} \tag{11}$$

is a complex quantity determined by the parameters

$$R = \frac{\chi_1}{\chi_2}; \quad q = \frac{K_1}{K_2}; \quad a = \epsilon_0 K_2 \chi_1, \tag{12}$$

where the resistivity and dielectric constant ratios R and q are dimensionless and a has the dimension of time.

Defining the complex electric fields $\boldsymbol{E}'_1$ and $\boldsymbol{E}'_2$, inside and outside the drop, such that

$$\boldsymbol{E}'_1 = -\nabla V'_1 \quad \text{and} \quad \boldsymbol{E}'_2 = -\nabla V'_2, \tag{13}$$

from equations (3), (9) and (10) it follows that the real parts of the electric field components at the drop surface ($r = b$) are given by

$$E_{1r} = 3E_0 \cos\theta\, \mathrm{Re}\,(A\,\mathrm{e}^{\mathrm{i}\omega t}); \tag{14a}$$

$$E_{2r} = -3E_0 \cos\theta\, \mathrm{Re}\,[(2A-1)\,\mathrm{e}^{\mathrm{i}\omega t}], \tag{14b}$$

$$E_{1\theta} = E_{2\theta} = -3E_0 \sin\theta\, \mathrm{Re}\,(A\,\mathrm{e}^{\mathrm{i}\omega t}), \tag{14c}$$

where $E_{1\theta}$, E_{1r} and $E_{2\theta}$, E_{2r} are the radial and transverse components of $\boldsymbol{E}'_1$ and $\boldsymbol{E}'_2$ respectively, the symbol Re denoting the operation of taking the real part of the complex values.

The expression for σ^* follows from equations (4*c*), (9), (10) and (11) so that, since $\sigma = \mathrm{Re}\,(\sigma^* \mathrm{e}^{\mathrm{i}\omega t})$, we obtain

$$\sigma = \frac{3\epsilon_0 K_2 E_0 (1-Rq)\cos\theta}{\sqrt{\{(2R+1)^2 + a^2\omega^2(q+2)^2\}}} \cos(\omega t - \alpha_\nu), \tag{15a}$$

where

$$\alpha_\nu = \tan^{-1}\left(\frac{a\omega(q+2)}{2R+1}\right); \quad 0 \leqslant \alpha_\nu \leqslant \tfrac{1}{2}\pi. \tag{15b}$$

Equation (15*a*) shows that the total charge on the surface is zero, that σ decreases with increasing frequency when all the other parameters remain fixed, and that the drop hemisphere facing the positive electrode becomes positively charged and that facing the negative electrode becomes negatively charged for $Rq > 1$ and vice versa for $Rq < 1$; when $Rq = 1$, $\sigma = 0$ over the whole surface. This is shown schematically in figure 1*b*.

The electric stress components at the interface are given by the well-known formulas (Jeans 1960):

$$F'_{r\nu} = \tfrac{1}{2}\epsilon_0 K_2\{E_{2r}^2 - E_{2\theta}^2 - q(E_{1r}^2 - E_{1\theta}^2)\}; \tag{16}$$

$$F'_{\theta\nu} = \epsilon_0 K_2 E_{2\theta}(E_{2r} - qE_{1r}), \tag{17}$$

$F'_{r\nu}$ and $F'_{\theta\nu}$ being the normal and transverse components of the electric stress, taken to be positive in the direction of increasing r and θ respectively.

Substituting equations (14) into equations (16) and (17) we obtain each stress as the sum of a steady component $F_{r\nu}$ or $F_{\theta\nu}$, and an alternating or time-dependent component, $F_{r\mathrm{T}}$ or $F_{\theta\mathrm{T}}$ of frequency 2ν, given by

$$F'_{r\nu} = F_{r\nu} + F_{r\mathrm{T}}, \tag{18}$$

$$F'_{\theta\nu} = F_{\theta\nu} + F_{\theta\mathrm{T}}, \tag{19}$$

where

$$F_{r\nu} = \tfrac{9}{4}\epsilon_0 K_2 E_0^2\left[\frac{(R^2 - 2qR^2 + 1) + a^2\omega^2(q-1)^2}{(2R+1)^2 + a^2\omega^2(q+2)^2}\right]\cos^2\theta + w_{\mathrm{S}}; \tag{20a}$$

$$F_{\theta\nu} = \tfrac{9}{2}\epsilon_0 K_2 E_0^2\left[\frac{R(Rq-1)}{(2R+1)^2 + a^2\omega^2(q+2)^2}\right]\sin\theta\cos\theta; \tag{20b}$$

$$F_{r\mathrm{T}} = \tfrac{9}{4}\epsilon_0 K_2 E_0^2[\mathrm{Re}(F_r^* \,\mathrm{e}^{2\mathrm{i}\omega t})]\cos^2\theta + w_{\mathrm{T}}; \tag{20c}$$

$$F_{\theta\mathrm{T}} = \tfrac{9}{2}\epsilon_0 K_2 E_0^2(Rq-1)\,[\mathrm{Re}\,(F_\theta^* \,\mathrm{e}^{2\mathrm{i}\omega t})]\sin\theta\cos\theta \tag{20d}$$

and w_{S} and w_{T} are steady and oscillatory θ-independent quantities given by

$$w_{\mathrm{S}} = \frac{9\epsilon_0 K_2 E_0^2(q-1)\,(R^2 + a^2\omega^2)}{4[(2R+1)^2 + a^2\omega^2(q+2)^2]}; \tag{21a}$$

$$w_{\mathrm{T}} = \tfrac{9}{8}\epsilon_0 K_2 E_0^2(q-1)\,[A^2\,\mathrm{e}^{2\mathrm{i}\omega t} + \bar{A}^2\,\mathrm{e}^{-2\mathrm{i}\omega t}], \tag{21b}$$

$\bar{A}$ being the complex conjugate of A, and

$$F_r^* = A^2(5-2q) - 2A + 1, \tag{22a}$$

$$F_\theta^* = \frac{R + \mathrm{i}a\omega}{[(2R+1) + \mathrm{i}a\omega(q+2)]^2}. \tag{22b}$$

From equation (20b) we observe that the steady transverse stress $F_{\theta\nu}$ at a given point on the drop surface changes sign at $Rq = 1$. This in turn influences the direction of the electrically induced flow on both sides of the interface, as will become clearer later when the velocity field is derived, so that when

$$\left.\begin{array}{lll} Rq > 1, & (F_{\theta\nu}/\cos\theta\sin\theta) > 0 & \text{and flow is } \textit{pole to equator};\\ Rq = 1, & F_{\theta\nu} = 0 & \text{and there is no flow;}\\ Rq < 1, & (F_{\theta\nu}/\cos\theta\sin\theta) < 0 & \text{and flow is } \textit{equator to pole}. \end{array}\right\} \tag{23}$$

These criteria, valid for $\nu \geqslant 0$ for the direction of flow and illustrated in figure 1b, are identical to those derived by Taylor (1966) for $\nu = 0$.

We wish now to show that the electric stress at $r = b$, derived by Allan & Mason (1962) and by Taylor (1966), for non-conducting and conducting media respectively, can be derived from equations (18) and (19), the only difference being that *mks* rather than *esu* units are employed here.

(i) $\chi_1, \chi_2 = \infty$: under these conditions the two phases are perfect dielectrics and $a = \infty$; it

follows also from equation (4*d*) that $\sigma = 0$. Equations (16) and (17) then become (we omit the details):

$$F'_{rv} = \tfrac{9}{4}\epsilon_0 K_2 E_0^2 \frac{(q-1)^2}{(q+2)^2}\left(\cos^2\theta + \frac{1}{q-1}\right)(1+\cos 2\omega t), \tag{24a}$$

$$F'_{\theta v} = 0. \tag{24b}$$

Equations (24) also follow from equations (20) by letting $a \to \infty$ and assuming that R remains bounded. The steady component $F_{r0}(= F'_{r0})$ for $\omega = 0$ and F_{rv} for $\omega > 0$ become from equation (24*a*)

$$F_{r0} = F_{rv} = \frac{9\epsilon_0 K_2 \bar{E}_0^2}{2}\frac{(q-1)^2}{(q+2)^2}\left(\cos^2\theta + \frac{1}{q-1}\right), \tag{25}$$

where $\bar{E}_0 = E_0/\sqrt{2}$ is the root-mean-square value of E for $\omega > 0$, and $\bar{E}_0 = E_0$ for $\omega = 0$. Equation (25) is equivalent to that used by Allan & Mason (1962).

(ii) $\nu = 0 (\omega = 0)$: here equations (18) and (19) reduce to:

$$F_{r0} = F'_{r0} = \frac{9\epsilon_0 K_2 E_0^2}{2(2R+1)^2}\{(R^2 - 2qR^2 + 1)\cos^2\theta + R^2(q-1)\}; \tag{26a}$$

$$F_{\theta 0} = F'_{\theta 0} = \frac{9\epsilon_0 K_2 E_0^2}{(2R+1)^2} R(Rq-1)\sin\theta\cos\theta, \tag{26b}$$

which are the electric stress components derived by Taylor (1966).

2.2 *Fluid motion inside and outside the drop*

The velocity field inside ($\boldsymbol{u}_1$) and outside ($\boldsymbol{u}_2$) the drop is generated by $F'_{\theta v}$, and by $F_{r\mathrm{T}}$ which induces oscillations of the drop surface and hence an oscillating flow; from the axial symmetry of both stresses it follows that $\boldsymbol{u}_j$ is axisymmetric about the direction of E.

The radial (W_r) and transverse (W_θ) velocity components of an axisymmetric flow field, when inertial effects are neglected, satisfy the linearized form of the Navier–Stokes equation and may be written (Goldstein 1938) in terms of the Stokes stream-function ψ as

$$W_r = \frac{1}{r^2\sin\theta}\frac{\partial\psi}{\partial\theta}, \quad W_\theta = \frac{-1}{r\sin\theta}\frac{\partial\psi}{\partial r}, \tag{27}$$

where ψ is the solution of

$$\left[\frac{\partial^2}{\partial r^2} + \frac{\sin\theta}{r^2}\frac{\partial}{\partial\theta}\left(\frac{1}{\sin^2\theta}\frac{\partial}{\partial\theta}\right)\right]^2 \psi = 0. \tag{28}$$

By trial we establish the following solution of equation (28):

$$\psi = (C_5 b^4 r^{-2} + C_6 b^2 + C_7 b^{-1} r^3 + C_8 b^{-3} r^5)\sin^2\theta\cos\theta, \tag{29}$$

where C_5, C_6, C_7 and C_8 are integration constants to be determined.

From equations (27) and (29) we obtain:

$$W_r = (C_5 b^4 r^{-4} + C_6 b^2 r^{-2} + C_7 b^{-1} r + C_8 b^{-3} r^3)(3\cos^2\theta - 1), \tag{30a}$$

$$W_\theta = (2C_5 b^4 r^{-4} - 3C_7 b^{-1} r - 5C_8 b^{-3} r^3)\sin\theta\cos\theta. \tag{30b}$$

The hydrodynamic stress components can be evaluated (Goldstein 1938) from the velocity field using the equations:

$$p_{rr} = -\mu(8C_5 b^4 r^{-5} + 6C_6 b^2 r^{-3} - 2C_7 b^{-1} + C_8 b^{-3} r^2)(3\cos^2\theta - 1), \tag{31a}$$

$$p_{r\theta} = -2\mu(8C_5 b^4 r^{-5} + 3C_6 b^2 r^{-3} + 3C_7 b^{-1} + 8C_8 b^{-3} r^2)\sin\theta\cos\theta, \tag{31b}$$

μ being the viscosity of the fluid.

PHILOSOPHICAL TRANSACTIONS OF THE ROYAL SOCIETY A MATHEMATICAL, PHYSICAL & ENGINEERING SCIENCES

To simplify the calculations we first determine the velocity field $\boldsymbol{u}_j^{\mathrm{I}}$ caused by $F'_{\theta\nu}$ and then $\boldsymbol{u}_j^{\mathrm{II}}$ caused by $F_{r\mathrm{T}}$, the total velocity field $\boldsymbol{u}_j$ being

$$\boldsymbol{u}_j = \boldsymbol{u}_j^{\mathrm{I}} + \boldsymbol{u}_j^{\mathrm{II}}, \tag{32}$$

because of linearity of equation (28).

(a) Flow due to $F'_{\theta\nu}$

The boundary conditions are taken to be:

$$\boldsymbol{u}_2^{\mathrm{I}} \to 0 \quad \text{at} \quad r \to \infty; \tag{33a}$$

$$\boldsymbol{u}_1^{\mathrm{I}} \text{ bounded} \quad \text{at} \quad r = 0; \tag{33b}$$

$$u_{1r}^{\mathrm{I}} = u_{2r}^{\mathrm{I}} = 0,\ u_{1\theta}^{\mathrm{I}} = u_{2\theta}^{\mathrm{I}} \quad \text{at} \quad r = b; \tag{33c}$$

$$F'_{\theta\nu} + p_{2r\theta}^{\mathrm{I}} - p_{1r\theta}^{\mathrm{I}} = 0 \quad \text{at} \quad r = b; \tag{33d}$$

where u_{1r}^{I}, $u_{1\theta}^{\mathrm{I}}$ and u_{2r}^{I}, $u_{2\theta}^{\mathrm{I}}$ are the radial and transverse components of the velocity field $\boldsymbol{u}_1^{\mathrm{I}}$ (inside) and $\boldsymbol{u}_2^{\mathrm{I}}$ (outside the drop), and $p_{1r\theta}^{\mathrm{I}}$, $p_{2r\theta}^{\mathrm{I}}$ are the transverse components inside and outside the drop of the hydrodynamic stress which balances $F'_{\theta\nu}$.

Applying equations (30) and (31*b*) to equations (33) we obtain for the velocity components:

$$u_{1r}^{\mathrm{I}} = U_\nu^{\mathrm{I}}(b^{-1}r - b^{-3}r^3)\,(3\cos^2\theta - 1), \tag{34a}$$

$$u_{1\theta}^{\mathrm{I}} = -U_\nu^{\mathrm{I}}(3b^{-1}r - 5b^{-3}r^3)\sin\theta\cos\theta, \tag{34b}$$

$$u_{2r}^{\mathrm{I}} = -U_\nu^{\mathrm{I}}(b^2r^{-2} - b^4r^{-4})\,(3\cos^2\theta - 1), \tag{34c}$$

$$u_{2\theta}^{\mathrm{I}} = 2U_\nu^{\mathrm{I}}b^4r^{-4}\sin\theta\cos\theta, \tag{34d}$$

while for the radial hydrodynamic stress components inside (p_{1rr}^{I}) and outside (p_{2rr}^{I}) the drop it follows from equations (31*a*), (33) and (34) that at $r = b$

$$p_{2rr}^{\mathrm{I}} - p_{1rr}^{\mathrm{I}} = -U_\nu^{\mathrm{I}}b^{-1}(2\mu_2 + 3\mu_1)\,(3\cos^2\theta - 1), \tag{35}$$

where μ_1 and μ_2 are the viscosities of the drop and of the medium respectively and

$$U_\nu^{\mathrm{I}} = U_{\mathrm{S}}^{\mathrm{I}} + U_{\mathrm{T}}^{\mathrm{I}}, \tag{36a}$$

$U_{\mathrm{S}}^{\mathrm{I}}$ and $U_{\mathrm{S}}^{\mathrm{I}}$ being the steady and oscillatory components of U_ν^{I} given by

$$U_{\mathrm{S}}^{\mathrm{I}} = \frac{9\epsilon_0 K_2 E_0^2 b}{20\mu_2(1+\lambda)} \frac{R(Rq-1)}{(2R+1)^2 + a^2\omega^2(q+2)^2} \tag{36b}$$

and

$$U_{\mathrm{T}}^{\mathrm{I}} = U_{\mathrm{S}}^{\mathrm{I}} \frac{\sqrt{(R^2 + a^2\omega^2)}}{R} \cos(2\omega t + \alpha_\nu^{\mathrm{I}}), \tag{36c}$$

where

$$\sin\alpha_\nu^{\mathrm{I}} = \frac{a\omega}{\sqrt{(R^2 + a^2\omega^2)}} \frac{(2R+1)\,(1 - 2qR - 2R) - a^2\omega^2(q+2)^2}{(2R+1)^2 + a^2\omega^2(q+2)^2}; \tag{36d}$$

$$\cos\alpha_\nu^{\mathrm{I}} = \frac{1}{\sqrt{(R^2 + a^2\omega^2)}} \frac{(2R+1)^2R - a^2\omega^2(q+2)\,(Rq - 2R - 2)}{(2R+1)^2 + a^2\omega^2(q+2)^2} \tag{36e}$$

define the value and sign of α_ν^{I} with $\lambda = \mu_1/\mu_2$ being the viscosity ratio.

(b) Flow due to $F_{r\mathrm{T}}$

In figure 1 we have defined the total deformation D'_ν in terms of the drop shape parameters d'_1 and d'_2. We write this as the sum of a steady component D_ν and an oscillatory component D_{T}:

$$D'_\nu = D_\nu + D_{\mathrm{T}}. \tag{37}$$

When D'_ν is small the equation of the drop surface is taken as

$$r = b\{1 + \tfrac{2}{3}(D_\nu + D_T)\,(3\cos^2\theta - 1)\}. \tag{38}$$

For simplicity let

$$D_T = \mathrm{Re}\,(H^*\,\mathrm{e}^{2\mathrm{i}\omega t}), \tag{39}$$

H^* being a time-independent complex quantity to be calculated, and neglect the effect of drop deformation on the fluid flow induced by the oscillations of the surface (justified since we are considering only a first order theory of D'_ν). From equation (38) we obtain

$$\partial r/\partial t = \tfrac{4}{3}b\omega(3\cos^2\theta - 1)\,\mathrm{Re}\,(\mathrm{i}H^*\,\mathrm{e}^{2\mathrm{i}\omega t}), \tag{40}$$

which represents the oscillating radial velocity of the surface ($r = b$).

If $\boldsymbol{u}_1^{II}$ and $\boldsymbol{u}_2^{II}$ are the velocity fields inside and outside the drop their boundary conditions are:

$$\boldsymbol{u}_2^{II} \to 0 \quad \text{as} \quad r \to \infty; \tag{41a}$$

$$\boldsymbol{u}_1^{II} \text{ bounded} \quad \text{at} \quad r = 0; \tag{41b}$$

$$u_{1r}^{II} = u_{2r}^{II} = \frac{\partial r}{\partial t}, u_{1\theta}^{II} = u_{2\theta}^{II} \quad \text{at} \quad r = b; \tag{41c}$$

$$p_{1r\theta}^{II} = p_{2r\theta}^{II} \quad \text{at} \quad r = b; \tag{41d}$$

where u_{1r}^{II}, $u_{1\theta}^{II}$ and u_{2r}^{II}, $u_{2\theta}^{II}$ are the radial and transverse components of the velocity inside and outside the drop and $p_{1r\theta}^{II}$, $p_{2r\theta}^{II}$ are the corresponding transverse components of the hydrodynamic stress in the two phases.

Imposing equations (41) on equations (30) and (31b) yields:

$$u_{1r}^{II} = U_T^{II}\{(16\lambda + 19)b^{-1}r - 3(2\lambda + 3)b^{-3}r^3\}\,(3\cos^2\theta - 1), \tag{42a}$$

$$u_{1\theta}^{II} = -U_T^{II}\{3(16\lambda + 19)b^{-1}r - 15(2\lambda + 3)b^{-3}r^3\}\sin\theta\cos\theta, \tag{42b}$$

$$u_{2r}^{II} = U_T^{II}\{(19\lambda + 16)b^2r^{-2} - 3(3\lambda + 2)b^4r^{-4}\}\,(3\cos^2\theta - 1), \tag{42c}$$

$$u_{2\theta}^{II} = -6U_T^{II}(3\lambda + 2)b^4r^{-4}\sin\theta\cos\theta, \tag{42d}$$

and for the radial components of the normal hydrodynamic stress at the drop surface both inside (p_{1rr}^{II}) and outside (p_{2rr}^{II}) the drop we derive from equation (31a) the following relations:

$$p_{2rr}^{II} - p_{1rr}^{II} = -U_T^{II}\mu_2 b^{-1}(19\lambda + 16)\,(2\lambda + 3)\,(3\cos^2\theta - 1), \tag{43}$$

where

$$U_T^{II} = \frac{2b\omega\,\mathrm{Re}\,(\mathrm{i}H^*\,\mathrm{e}^{2\mathrm{i}\omega t})}{15(1 + \lambda)} \tag{44}$$

is an oscillatory quantity.

Thus $\boldsymbol{u}_j^{II}$ is an oscillating velocity field with no steady components and is given by equations (42) and (44) once H^* is known; this is evaluated later from the balance of the normal stresses at the interface.

2.3. *Steady deformation*

The sum ($f_{r\nu}$) of the steady electric and hydrodynamic normal stresses at the interface is balanced by the interfacial tension as a result of changes in surface curvature accompanying deformation of the drop so as to satisfy the capillary equation

$$\gamma(b_1^{-1} + b_2^{-1}) = f_{r\nu}, \tag{45}$$

where b_1 and b_2 are the steady principal radii of curvature at any point of the deformed drop surface and γ is the interfacial tension.

Adding the time-independent parts of equations (18) and (35) (the flow induced by the oscillating drop does not produce any time-independent normal stress at $r = b$) we obtain on reduction

$$f_{rv} = \tfrac{9}{4}\epsilon_0 K_2 E_0^2 \Phi_v \cos^2\theta + \text{constant}, \tag{46}$$

where
$$\Phi_v = 1 - \frac{R(11\lambda+14) + R^2[15(\lambda+1) + q(19\lambda+16)] + 15a^2\omega^2(1+\lambda)(1+2q)}{5(1+\lambda)[(2R+1)^2 + a^2\omega^2(q+2)^2]}. \tag{47}$$

For $D_T = 0$ and $D_v \ll 1$, b_1 and b_2 can be calculated using equation (38), so that substituting equation (46) into equation (45) yields on reduction:

$$D_v = \frac{9\epsilon_0 K_2}{16\gamma}\Phi_v(\bar{E}_0^2 b). \tag{48}$$

We note that by using $\bar{E}_0$ the case $v = 0$ is included in equation (48), as can be proved by letting $\omega = 0$ in equation (35), adding it to equation (26*a*) and requiring that the resulting total radial stress is balanced by the interfacial tension so as to satisfy equation (45). Following the terminology of Taylor (1966), Φ_v is a discriminating function which determines the type of deformation: the drop becomes (i) a prolate spheroid ($D_v > 0$) when $\Phi_v > 0$ and (ii) an oblate spheroid ($D_\tau < 0$) when $\Phi_v < 0$.

Equation (47) shows that Φ_v varies with ω. When $\Phi_v = 0$ the mean drop shape is spherical whatever the field; if $D_T \neq 0$, the drop oscillates about the spherical shape. This occurs at a critical frequency v_c corresponding to $\Phi_{v_c} = 0$ in equation (47):

$$v_c = \frac{\sqrt{\{R^2[q(19\lambda+16) - 5(1+\lambda)] - 3R(3\lambda+2) - 5(1+\lambda)\}}}{2a\pi|q-1|\sqrt{\{5(1+\lambda)\}}}. \tag{49}$$

It follows from equation (49) that v_c exists when

$$Rq \geqslant 1 + \frac{5(1+\lambda)}{16+19\lambda}\frac{(R-1)^2}{R}; \tag{50}$$

also when $q = 1$, $v_c = \infty$.

When the equality in equation (50) is satisfied:

$$v_c = 0; \quad \Phi_0 = 0; \quad D_0 = 0. \tag{51}$$

It follows from equation (48) that

(i) when $Rq > 1$

$$\partial D_v/\partial v > 0, \tag{52}$$

the deformation increasing with frequency, and vice versa for $Rq < 1$, and

(ii) when $Rq = 1$

$$D_v = \frac{9\epsilon_0 K_2}{16\gamma}\frac{(q-1)^2}{(q+2)^2}\bar{E}_0^2 b, \tag{53}$$

which is independent of the frequency. Equation (53) was also derived by Allan & Mason (1962) for $\chi_1, \chi_2 = \infty$. This coincidence occurs because, as already discussed, $\sigma = 0$ for leaky dielectrics with $Rq = 1$ and for perfect dielectrics.

When the equalities are satisfied equations (50) and (52) define two curves in the (R, q) plane which are tangent at $R = q = 1$ and which divide the plane into three regions, each characterizing

PHILOSOPHICAL TRANSACTIONS OF THE ROYAL SOCIETY A MATHEMATICAL, PHYSICAL & ENGINEERING SCIENCES

a class of systems with common modes of deformation summarized below and illustrated in figure 2.

Class A: $$Rq \leqslant 1, \quad \partial D_\nu/\partial \nu \leqslant 0; \quad D_\nu \geqslant 0; \tag{54a}$$

class B: $$1 < Rq < 1+\frac{5(1+\lambda)}{16+19\lambda}\frac{(R-1)^2}{R}, \quad \partial D_\nu/\partial \nu > 0, \quad D_\nu > 0; \tag{54b}$$

class C: $$Rq \geqslant 1+\frac{5(1+\lambda)}{16+19\lambda}\frac{(R-1)^2}{R}, \quad \frac{\partial D_\nu}{\partial \nu} > 0 \begin{cases} D_\nu \leqslant 0 & \text{if} \quad \nu \leqslant \nu_c, \\ D_\nu > 0 & \text{if} \quad \nu > \nu_c. \end{cases} \tag{54c, 54d}$$

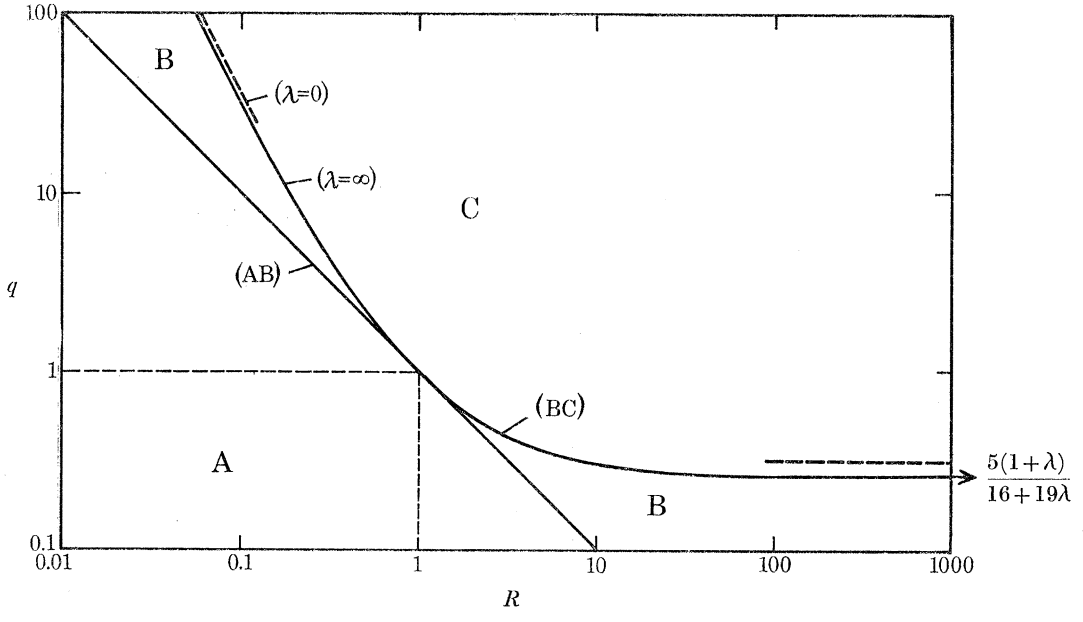

FIGURE 2. Loci defined by equations (54) characterizing sets of systems whose modes of steady deformation are illustrated in the table below. The equations (54) giving the two curves (AB) and (BC) given by equations (54) show that for large values of R, (BC) tends to a horizontal asymptote $q = 5(1+\lambda)/(16+19\lambda)$, whereas (AB) tends to $q = 0$. For both curves $q \to \infty$ as $R \to 0$. We adopt the convention, contained in equations (54), that points on the lines (AB) and (BC) fall in classes A and C respectively.

	A	B	C
$\partial D_\nu/\partial \nu$	$\leqslant 0$	> 0	> 0
D_ν	> 0	> 0	$\leqslant 0 (\nu \leqslant \nu_c)$
			$> 0 (\nu > \nu_c)$

Curves (AB) and (BC) in figure 2 have the common limit $q \to \infty$ for $R \to 0$; however, when $R \to \infty$, $q \to 0$ on curve (AB), and $q \to 5(1+\lambda)/(16+19\lambda)$ on curve (BC).

Thus the mode of deformation of a system is determined by the parameters R, q and λ; the effect of λ, however, is small as indicated in figure 2 by the dashed ($\lambda = 0$) and continuous ($\lambda = \infty$) lines (BC).

Φ_ν is a monotonic function of ν as is shown by values calculated from equation (47) in figure 3 for systems belonging to classes A, B, and C. For $\nu = 0$ equation (47) reduces to

$$\Phi_0 = \frac{1}{(2R+1)^2}\left(R^2+1+\frac{3R(2+3\lambda)}{5(1+\lambda)} - qR^2\frac{16+19\lambda}{5(1+\lambda)}\right), \tag{55}$$

which is the expression derived by Taylor (1966), corrected for a small arithmetic error in deriving the hydrodynamic stress (Melcher & Taylor (1969)). For all the parameters fixed and $\nu \to \infty$ equation (47) reduces to

$$\Phi_\infty = \frac{(q-1)^2}{(q+2)^2}, \tag{56}$$

which corresponds to the expression derived by Allan & Mason (1962) for perfect dielectrics (equation (53)) for the reason already mentioned.

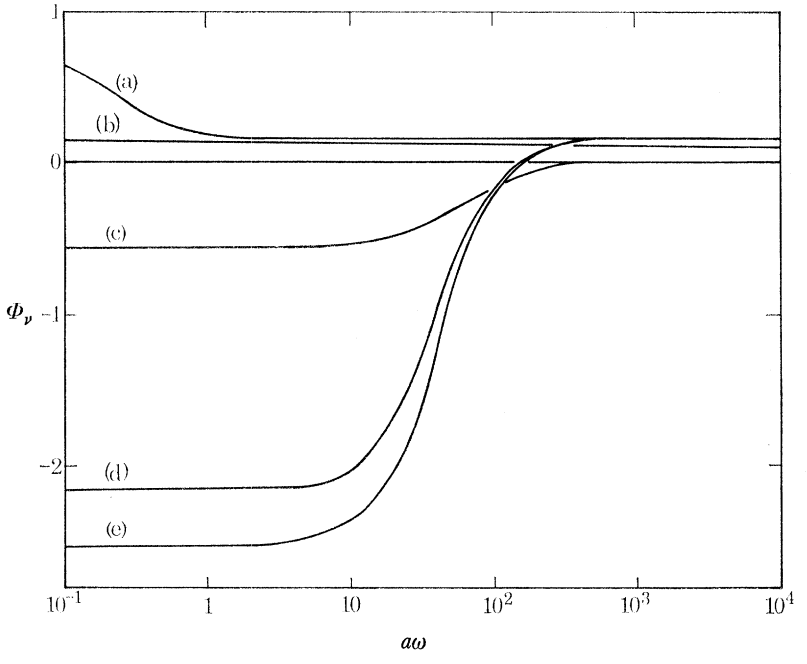

FIGURE 3. Variation of Φ_ν with $a\omega$ calculated from equation (47). The curves are drawn for values of the electrical variables (shown in the following table) which are representative of the three classes of systems defined in equations (54). The limiting values of Φ_ν are Φ_0 and Φ_∞ at $(a\omega) \to 0, \infty$ respectively.

class	R	q	λ	Φ_0	Φ_∞	av_c
A(a)	0.1	3	0.1	0.64	0.16	—
B(b)	10	0.2	0.1	0.11	0.13	—
C(c)	100	1	0.1	−0.55	0	∞
C(d)	100	3	0.1	−2.16	0.16	24
C(e)	100	3	10	−2.54	0.16	26

2.4. *Oscillatory and total deformations*

The total oscillating normal stress f_{rT} at the drop surface can be balanced by interfacial forces through a time-dependent change in curvature (i.e. an oscillation) of the interface. This change in curvature must again satisfy equation (45) where b_1 and b_2 are now the time-dependent principal radii of curvature.

By adding the time-dependent parts of equations (18), (35) and (43) we obtain

$$f_{rT} = \mathrm{Re}\{[\tfrac{9}{4}\epsilon_0 K_2 E_0^2 (F_{r2}^* - \lambda_1 F_{\theta 2}^*) - 8\omega\mu_2\lambda_2 \mathrm{i} H^*]\, \mathrm{e}^{2\mathrm{i}\omega t}\} \cos^2\theta + \text{const.} \tag{57}$$

where

$$\lambda_1 = \frac{3(2+3\lambda)}{5(1+\lambda)} \quad \text{and} \quad \lambda_2 = \frac{(19\lambda+16)\,(2\lambda+3)}{20(1+\lambda)}. \tag{58}$$

Substituting equation (57) into equation (45) and calculating the time-dependent principal radii of curvature from equation (38) with $D_\nu = 0$ and D_T ($\ll 1$) given by equation (39) we obtain

$$H^* = \frac{9\epsilon_0 K_2 E_0^2 b}{32\gamma} h^*, \tag{59}$$

where

$$h^* = \frac{F_{r2}^* - \lambda_1 F_{\theta 2}^*}{1 + ik\lambda_2}, \tag{60}$$

$$k = \omega\mu_2 b/\gamma. \tag{61}$$

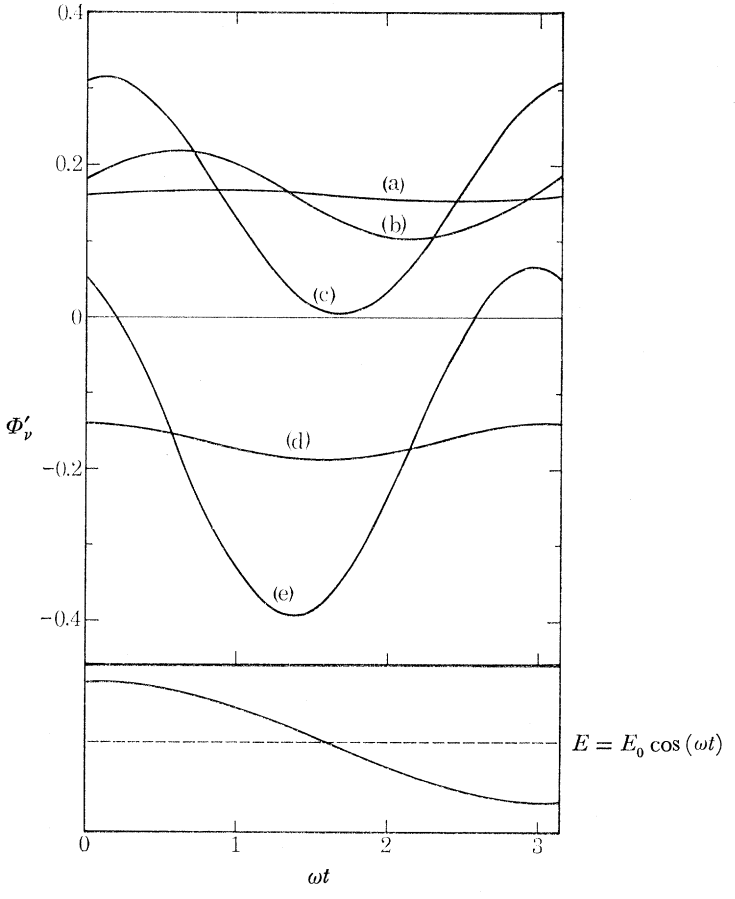

FIGURE 4. The time-dependent total discriminating function Φ'_ν, defined by equation (65) calculated for $R = 100$, $q = 3$ and $\lambda = 0.1$ when (i) $a\omega = 10^4$ and: $k = 10$ (curve a), $k = 1$ (curve b), $k = 0.1$ (curve c); and (ii) $a\omega = 10^2$ and: $k = 10$ (curve d), $k = 1$ (curve e). At the bottom of the figure, the graph of $E = E_0 \cos \omega t$ shows that the drop oscillates twice as fast as the field, the phase angle being determined by equations (63*a*).

Substituting equation (59) into equation (39) yields

$$D_T = \frac{9\epsilon_0 K_2}{32\gamma} \frac{I \cos(2\omega t + \alpha_\nu^{II})}{\sqrt{(1 + k^2\lambda_2^2)}} (E_0^2 b), \tag{62}$$

where

$$\cos \alpha_\nu^{II} = \frac{h^* + \bar{h}^*}{2I}, \quad \sin \alpha_\nu^{II} = \frac{h^* - \bar{h}^*}{2Ii} \tag{63a}$$

and

$$I = \left\{ \Phi_\nu^2 + \frac{a^2\omega^2(1 - Rq)^2(19\lambda + 16)\,[20q(1 + \lambda) - (\lambda + 4)]}{25(1 + \lambda)^2[(2R + 1)^2 + a^2\omega^2(q + 2)^2]^2} \right\}^{\frac{1}{2}}, \tag{63b}$$

$\bar{h}^*$ being the complex conjugate of h^*.

PHILOSOPHICAL TRANSACTIONS OF THE ROYAL SOCIETY A MATHEMATICAL, PHYSICAL & ENGINEERING SCIENCES

Thus from equations (37), (48) and (62) it follows that

$$D'_\nu = \frac{9\epsilon_0 K_2}{32\gamma}\Phi'_\nu(E_0^2 b), \tag{64}$$

where

$$\Phi'_\nu = \Phi_\nu + \frac{I\cos(2\omega t + \alpha_\nu^{\mathrm{II}})}{\sqrt{(1+k^2\lambda_2^2)}} \tag{65}$$

is the total discriminating function.

To examine the conditions under which the oscillatory deformation is much smaller than the steady value we consider the ratio:

$$\frac{D_{\mathrm{T}}}{D_\nu} = \frac{I\cos(2\omega t + \alpha_\nu^{\mathrm{II}})}{\Phi_\nu\sqrt{(1+k^2\lambda_2^2)}} \tag{66}$$

obtained from equations (48) and (62). The dimensionless parameter k, defined by equation (61) and which plays an important part in characterizing the ratio (D_{T}/D_ν), may be considered as the ratio of the oscillatory hydrodynamic stress $(\omega\mu_2)$ and the capillary pressure (γ/b) at the drop interface. When $(\omega\mu_2) \to \infty$ and (γ/b) remains fixed, $k \to \infty$ and $(D_{\mathrm{T}}/D_\nu) \to 0$, the drop surface being unable to respond to the oscillating stress $F_{r\mathrm{T}}$.

Figure 4 shows the calculated relation between Φ'_ν and (ωt) given by equation (65). It shows that for large values of k the amplitude of the oscillation of the drop surface is small (curves a, d) and that as k decreases D_{T} increases (curves b, c) until it becomes larger than D_ν (curve e), the drop oscillating from a prolate to an oblate spheroid. The drop oscillates twice as fast as the field E (plotted at the bottom of figure 4) and is generally out of phase with it; when $k \to 0$ the maximum and minimum deformations tend to occur at $E = E_0$ and $E = 0$ respectively (curves c, e).

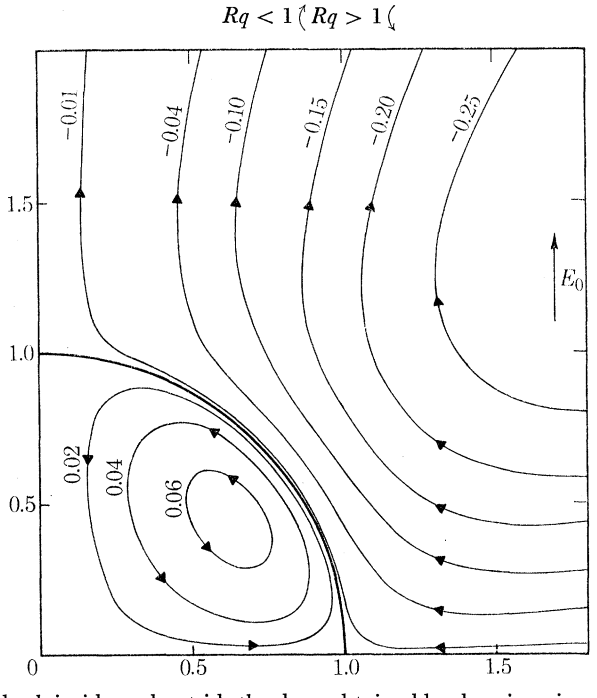

FIGURE 5. Steady flow field both inside and outside the drop obtained by drawing nine streamlines whose equations were derived from equations (34) for $b = 1$. The flow pattern is shown only for the first quadrant, being identical in the other three because of symmetry, the streamlines being characterized by a constant proportional to ψ. For $Rq < 1$ the flow is equator-to-pole, whereas for $Rq > 1$ it is pole-to-equator. This figure is identical to that given by Taylor (1966) because the presence of the term $(a\omega)$ in equations (34) does not change the flow pattern even if it does change the absolute values of the velocity components (equation (36b)). The effect of changing the value of Rq (< 1 or > 1) on the flow direction is illustrated schematically on the top of the figure.

2.5. *Fluid circulation*

Substituting equation (59) into equation (44) yields:

$$U_{\mathrm{T}}^{\mathrm{II}} = -\frac{3\epsilon_0 K_2 E_0^2 b}{80\mu_2(1+\lambda)} \frac{Ik}{\sqrt{(1+k^2\lambda_2^2)}} \sin(2\omega t + \alpha_\nu^{\mathrm{II}}). \tag{67}$$

Inspection of equation (67) shows that the velocity field $\boldsymbol{u}_j^{\mathrm{II}}$ is 90° out of phase with D_{T} (equation (62)) and that its amplitude is a complicated function of R, q, λ, k and $(a\omega)$, its value remaining finite as $(a\omega)$ increases to infinity.

Thus the complete velocity field $\boldsymbol{u}_j$ is determined, its velocity components being given by adding equations (34) to (42). The steady components of $\boldsymbol{u}_j$ are given by equations (34) in which U_ν^{I} is replaced by $U_{\mathrm{S}}^{\mathrm{I}}$ given in equation (36*b*) with $(2\bar{E}_0^2)$ replacing E_0^2 so as to include the case of $\nu = 0$. The pattern of the flow is identical to that derived by Taylor (1966) for $\nu = 0$ to which equations (34) reduce for $\nu = 0$. The effect of increasing ν is to decrease the steady velocity components so that the steady electrohydrodynamic flow dies out at high ν. The calculated steady streamlines are given in figure 5 and are identical to those given by Taylor (1966) for $\nu = 0$.

2.6. *Further considerations*

(*a*) *Conductive drops in perfect dielectrics*

Of the several further cases of physical importance which can be envisaged in terms of limiting values of the electric and other parameters, we will consider only that for which

$$\chi_2 = \infty, \quad R = 0. \tag{68}$$

Substituting equation (68) into equation (15*a*) gives

$$\sigma = \frac{3\epsilon_0 K_2 E_0 \cos\theta}{\sqrt{(1+a^2\omega^2(q+2)^2)}} \cos[\omega t - \tan^{-1} a\omega(q+2)], \tag{69}$$

where $0 \leqslant \tan^{-1} a\omega(q+2) \leqslant \frac{1}{2}\pi$. Equation (69) for $\nu = 0$ reduces to the well-known formula (Allan & Mason 1962)

$$\sigma = 3\epsilon_0 K_2 E_0 \cos\theta. \tag{70}$$

From equations (20*b*) and (68) we obtain $F_{\theta\nu} = 0$ and hence the steady component of the velocity field vanishes, whereas from equations (48) and (68) we obtain

$$D_\nu = \frac{9\epsilon_0 K_2}{16\gamma} \frac{1+a^2\omega^2(q-1)^2}{1+a^2\omega^2(q+2)^2} (\bar{E}_0^2 b), \tag{71}$$

which reduces when the drop is a perfect conductor ($\chi_1 = 0$ hence $a = 0$) to

$$D_\nu = \frac{9\epsilon_0 K_2}{16\gamma} (\bar{E}_0^2 b), \tag{72}$$

which has been already calculated (Allan & Mason 1962) and which is independent of ν.

Inspection of equation (71) shows that $D_\nu > 0$ and $(\partial D_\nu/\partial\nu) < 0$ also predicted from equations (54) since the system belongs to class A.

(*b*) *Surface conductance and convection of charge*

In deriving the theory we have neglected the effect of the motion of charge on the drop surface which is caused by a combination of surface conductance and surface flow, the latter caused by the unbalanced transverse electric stress $F'_{\theta\nu}$ and by the oscillating drop surface. We may write this total flow of charge per unit length of surface as

$$Q_{\mathrm{S}} = E_{2\theta}/\chi_{12} + \sigma u_{2\theta}, \tag{73}$$

where χ_{12} is the surface resistivity and the other quantities are evaluated at $r = b$.

When Q_S is taken into account the rate of increase of σ is augmented by $-\nabla_2 Q_S$ (∇_2 is the two-dimensional divergence on the drop surface) so that the boundary conditions for the electric potentials, given in complex form in equations (4), reduce, in real form, to

$$V_2 \to -Er\cos\theta \quad \text{as} \quad r \to \infty, \tag{74a}$$

$$V_1 = V_2 \quad \text{at} \quad r = b, \tag{74b}$$

$$\epsilon_0 K_2 \frac{\partial V_2}{\partial r} - \epsilon_0 K_1 \frac{\partial V_1}{\partial r} = -\sigma \quad \text{at} \quad r = b, \tag{74c}$$

$$\frac{1}{\chi_2}\frac{\partial V_2}{\partial r} - \frac{1}{\chi_1}\frac{\partial V_1}{\partial r} - \nabla_2 Q_S = \frac{\partial \sigma}{\partial t} \quad \text{at} \quad r = b, \tag{74d}$$

$$V_1 \text{ bounded} \quad \text{at} \quad r = 0. \tag{74e}$$

Thus the solution for V_1 and V_2 is complicated by Q_S which itself is an unknown function of V_1 and V_2. However, since we wish to find the limits of validity of the theory based on the assumption $\nabla_2 Q_S = 0$ we may take the latter to be very small so that as a first-order approximation we can evaluate $\nabla_2 Q_S$ by inserting in equation (73) the values of $E_{2\theta}$, σ and $u_{2\theta}$ given in equations (14c), (15a), (34d) and (42d) and hence derive the conditions

$$|\nabla_2 Q_S| \ll \left|\frac{1}{\chi_1}\frac{\partial V_1}{\partial r}\right| \quad \text{or} \quad |\nabla_2 Q_S| \ll \left|\frac{1}{\chi_2}\frac{\partial V_2}{\partial r}\right|, \tag{75}$$

which represent the restrictions under which the theory applies. We will return to this point later.

In the experiments described below, quantitative confirmation of equations (48), (49), (55), (56) and (72), and qualitative confirmation of equations (23), (62) and (66) were obtained.

3. Experimental part

The experiments were performed using 22 different systems consisting of various combinations of two immiscible phases selected from the liquids listed at the bottom of table 1; the medium (phase 2) was chosen to have a high viscosity and/or nearly the same density as the drop (phase 1) so as to effectively eliminate sedimentation.

The electric fields were applied in a rectangular glass cell which had two transparent and flat glass electrodes (Corning Glass) cemented to the inner walls, to allow viewing either normal or parallel to the direction of the electric field. The dimensions of the electrodes were 4×4 cm (about 0.3 cm in thickness), and the gap in between them was about 1.7 cm. The drops were sufficiently small ($b = 0.02$ to 0.1 cm) that they could be considered to be subjected to a uniform electric field when lying in the central region of the condenser gap.

The electric fields were applied across the electrodes from stabilized power supplies: (i) 0 to 10 kV ($\nu = 0$), (ii) 0 to 15 kV ($\nu = 60$ Hz sine wave), and (iii) 0 to 8 kV (ν from 0 to 10 Hz, square wave, the only design available to us) which was obtained by a connexion in series of a pulsed square-wave and a d.c. power supply. The frequency, electric potential and wave form were measured before each experiment by means of an oscilloscope.

The events were viewed through a microscope along and/or perpendicular to the field direction and were generally photographed with a Nikon 35 mm camera attached to the microscope or by cinematography, at speeds up to 1000 pictures per second with a Hycam cine-camera.

The flow patterns were visualized by adding tiny guanine crystals (Mearl Corp., Ossining, N.Y.) to the suspending and suspended phases; the experiments were conducted in a room whose temperature was controlled at 22 ± 1 °C; the values of the conductivities and dielectric constants

of the systems were taken to be those reported by Allan & Mason (1962) and were assumed constant for all the silicone oils and for the watery phases; the viscosities were measured with a rotational viscometer (Epprecht Rheomat) and the interfacial tensions were measured by the shear-deformation method (Rumscheidt & Mason 1961) or by the ring method (Cenco).

TABLE 1. PROPERTIES OF THE SYSTEMS

system	phase 1/2	γ / dyn cm^{-1}	μ_2/P	λ	K_2	q	χ_1/Ωm	a/s	R
class A_1									
1	N M_3	5.5	54	1.2	2.77	2.3	1×10^{9}	2.4×10^{-2}	$<3\times10^{-2}$
2	T M_3	3.9	54	3.2	2.77	2.2	2.2×10^{9}	5.4×10^{-2}	$<7\times10^{-2}$
3	Z M_3	3.0	54	0.2	2.77	1.9	2.8×10^{9}	6.9×10^{-2}	$<9\times10^{-2}$
4	N M_6	5.5	1210	5×10^{-2}	2.77	2.3	1×10^{9}	2.4×10^{-2}	$<3\times10^{-2}$
5	T M_6	3.9	1210	0.14	2.77	2.2	2.2×10^{9}	5.4×10^{-2}	$<7\times10^{-2}$
6	Z M_6	3.0	1210	8×10^{-3}	2.77	1.9	2.8×10^{9}	6.9×10^{-2}	$<9\times10^{-2}$
class A_2									
7	Y_1 N	13	65	1×10^{-4}	6.30	12.7	1×10^{4}	5.6×10^{-7}	1×10^{-5}
8	Y_2 N	3.0	65	1×10^{-4}	6.30	12.7	1×10^{4}	5.6×10^{-7}	1×10^{-5}
9	Y_1 T	26	174	6×10^{-5}	6.04	13.2	1×10^{4}	5.3×10^{-7}	4.5×10^{-4}
10	Y_2 T	7.6	174	6×10^{-5}	6.04	13.2	1×10^{4}	5.3×10^{-7}	4.5×10^{-4}
11	Y_1 M_3	30	54	2×10^{-4}	2.77	29	1×10^{4}	2.4×10^{-7}	$<3\times10^{-6}$
12	Y_2 M_3	9.0	54	2×10^{-4}	2.77	29	1×10^{4}	2.4×10^{-7}	$<3\times10^{-6}$
13	Y_1 M_6	30	1210	8×10^{-6}	2.77	29	1×10^{4}	2.4×10^{-7}	$<3\times10^{-6}$
14	Y_2 M_6	9.0	1210	8×10^{-6}	2.77	29	1×10^{4}	2.4×10^{-7}	$<3\times10^{-6}$
class C									
15	M_2 N	5.5	65	0.15	6.30	0.44	$>3\times10^{10}$	>1.67	>30
16	M_3 N	5.5	65	0.83	6.30	0.44	$>3\times10^{10}$	>1.67	>30
17	M_4 N	5.5	65	1.85	6.30	0.44	$>3\times10^{10}$	>1.67	>30
18	M_1 T	3.9	174	3×10^{-2}	6.04	0.46	$>3\times10^{10}$	>1.60	>14
19	M_2 T	3.9	174	6×10^{-2}	6.04	0.46	$>3\times10^{10}$	>1.60	>14
20	M_5 T	3.9	174	1.34	6.04	0.46	$>3\times10^{10}$	>1.60	>14
21	M_1 Z	3.0	10	0.5	5.33	0.52	$>3\times10^{10}$	>1.41	>107
22	M_2 Z	3.0	10	5.4	5.33	0.52	$>3\times10^{10}$	>1.41	>107

Liquids

M_1, M_5, M_6	silicone oils 510F	$\rho = 1.00$ g/cm^3	$\mu = 5$; $\mu = 234$; $\mu = 1210$ P (Dow Corning)
M_2, M_3, M_4	silicone oils 200F	$\rho = 0.98$ g/cm^3	$\mu = 10$; $\mu = 54$; $\mu = 120$ P (Dow Corning)
N	oxidized castor oil	$\rho = 0.98$ g/cm^3	$\mu = 65$ P (Baker Castor Oil Co., N.Y.)
T	sextolphthalate	$\rho = 1.04$ g/cm^3	$\mu = 174$ P (Howard & Sons Ltd, Canada)
Z	Ucon oil LB–1715	$\rho = 1.04$ g/cm^3	$\mu = 10$ P (Union Carbide)
Y_1; Y_2	distilled water; distilled water + 1% vol. Tween 20 (Atlas)		

In the Theoretical Part we have employed SI units, except for writing the permittivities of the phases as the product $K_1\epsilon_0$ and $K_2\epsilon_0$ of the dielectric constants K_1, K_2 and the permittivity of free space ϵ_0 (Harnwell 1949). However, in presenting the experimental results we have used practical units, for example the poise ($1\,\mathrm{P} = 10^{-1}\,\mathrm{kg\,m^{-1}\,s^{-1}}$) for the viscosity, and (kV/cm) instead of (V/m) for the field intensity.

4. RESULTS AND DISCUSSION

4.1. *Steady deformation*

The equations derived in the Theoretical Part predict a steady deformation having the form:

$$D_v = m_v(\bar{E}_0^2 b), \tag{76}$$

where

$$m_v = (9\epsilon_0 K_2/16\gamma)\,\Phi_v. \tag{77}$$

PHILOSOPHICAL TRANSACTIONS OF THE ROYAL SOCIETY A MATHEMATICAL, PHYSICAL & ENGINEERING SCIENCES

Over the range 0 to 5 kV/cm of $\bar{E}_0$ and with different values of b for each system, the measured D_0 and D_{60} of the 22 systems listed in table 1 showed a linear variation with $(\bar{E}_0^2 b)$ as predicted by the theory. Experimental values m_ν^* were evaluated by the method of least squares (table 2). It was found that the systems fell into classes A and C (equations (54), figure 2); those belonging to class A were further subdivided into A_1 and A_2 in which $m_0 > m_{60}$ and $m_0 \simeq m_{60}$ respectively. An example of each class is shown by the linear plots in figure 6.

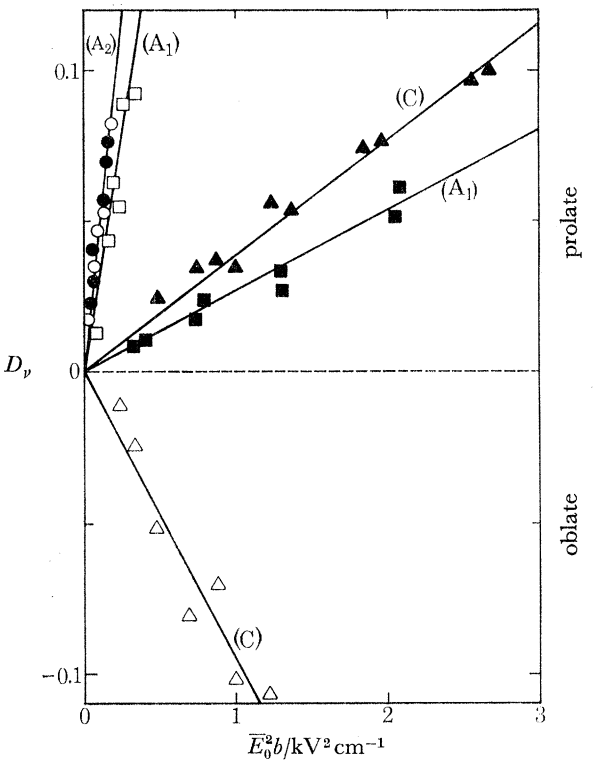

FIGURE 6. Linear variation of D with $(\bar{E}_0^2 b)$ showing the three modes of deformation which characterize the three classes of systems shown in table 1. The deformations at $\nu = 0$ (open points) and at $\nu = 60$ Hz (closed points) are shown for system 1 (square points, A_1), system 7 (circular points, A_2) and system 16 (triangular points, C). A positive slope indicates deformation to a prolate spheroid and a negative slope deformation to an oblate spheroid. The continuous lines have been fitted by the method of least squares.

(*a*) *Class* A_1: *systems* 1 *to* 6

Here $Rq < 1$; $1 \times 10^9 \leqslant \chi_1 \leqslant 2.8 \times 10^9$, the suspending phase in all the systems being a silicone oil.

Φ_0 is given by equation (55); Φ_{60} is given approximately by equation (56) to which equation (47) reduces under the condition $a\omega \to \infty$. Thus from equation (77) m_0 and m_{60} can be calculated and compared with the experimental values m_0^* and m_{60}^* (table 2). As predicted $m_0 > m_{60} > 0$, the drop deforming into prolate spheroids which are more elongated for $\nu = 0$ than for $\nu = 60$ Hz; however the ratios m_0^*/m_0 and m_{60}^*/m_{60} fell between 1.0 and 3.3; 1.6 and 4.2 respectively. Possible reasons for this discrepancy are discussed later.

(*b*) *Class* A_2: *systems* 7 *to* 14

Here $Rq < 1$; $\chi_1 \simeq 1 \times 10^4$, the drop being water or water containing a surfactant to lower γ, and $(a\omega) \simeq 0$ when $\nu \leqslant 60$ Hz. Thus equation (55) gives $\Phi_0 = \Phi_{60}$ and, since $R \simeq 0$ for these systems, $D_0 \simeq D_{60}$ is given by equation (72) and $\Phi_0 = \Phi_{60} \simeq 1$ (equation (55)).

The comparison between experimental results and theory (table 2) shows that, as predicted, $m^*_{60} \simeq m^*_0$. However, the ratios m^*_{60}/m_{60} and m^*_0/m_0 again fell between 1.4 and 4.4; 1.7 and 3.9 respectively.

(*c*) *Class C*: *systems* 15 *to* 22

Here $Rq > 1$; $\chi_1 > 3 \times 10^{10}$, the drop being a silicone oil. Equation (55) gives Φ_0 and equation (47) gives Φ_ν; however for $\nu = 60$ Hz it can be seen that Φ_{60} is again given approximately by equation (56) since a is large and hence $(a\omega) \to \infty$. Table 2 shows that the predicted signs of the deformations were always experimentally verified, the systems showing oblate spheroidal deformations at $\nu = 0$ ($D_0 < 0$) and prolate spheroidal deformations at $\nu = 60$ Hz ($D_{60} > 0$) as illustrated by the series of photographs in figure 7, plate 6.

TABLE 2. COMPARISON OF OBSERVED AND CALCULATED DEFORMATIONS

system†	m_0	m^*_0	m_{60}	m^*_{60}	m^*_0/m_0	m^*_{60}/m_{60}	$(E_0)_{max}$/kV cm^{-1}‡ $\nu = 0$	$(E_0)_{max}$/kV cm^{-1}‡ $\nu = 60$ Hz
	kV^{-2} cm							
class A_1								
1	0.24	0.39	0.02	0.03	1.6	1.5	27	120
2	0.31	1.31	0.03	0.04	4.2	1.3	29	241
3	0.38	0.91	0.03	0.10	2.4	3.3	15	206
4	0.23	0.88	0.02	0.02	3.8	1.0	85	458
5	0.30	0.90	0.03	0.03	3.0	1.0	73	726
6	0.38	0.93	0.02	0.06	2.4	3.0	64	941
class A_2								
7	0.24	0.51	0.24	0.51	2.1	2.1	2×10^3	17
8	1.05	2.04	1.05	2.20	1.0	2.1	2×10^3	17
9	0.12	0.36	0.12	0.35	3.0	2.9	4×10^3	19
10	0.40	1.58	0.40	1.67	3.9	4.2	4×10^3	19
11	0.05	0.19	0.05	0.22	3.8	4.4	5×10^3	6
12	0.15	0.25	0.15	0.26	1.7	1.7	5×10^3	6
13	0.05	0.19	0.05	0.16	3.8	3.2	23×10^3	30
14	0.15	0.35	0.15	0.29	2.3	1.9	23×10^3	30
class C								
15	−0.06	−0.07	0.03	0.03	1.2	1.0	8	13
16	−0.07	−0.10	0.03	0.03	1.4	1.0	9	13
17	−0.08	−0.13	0.03	0.04	1.6	1.3	12	13
18	−0.09	−0.17	0.04	0.06	1.9	1.5	13	32
19	−0.09	−0.19	0.04	0.05	2.1	1.2	13	32
20	−0.12	−0.33	0.04	0.09	2.7	2.2	19	30
21	−0.17	−0.19	0.03	0.06	1.1	2.0	3	9
22	−0.21	−0.24	0.03	0.03	1.1	1.0	6	9

† Systems defined in table 1.

‡ Calculated from equation (83).

Note. The maximum standard deviation of m^*_ν from the least mean square regression line was 10 %.

According to the theory, systems using this group should exhibit a critical frequency ν_c at which $D_{\nu_c} = 0$. Thus using system 18 and square-wave variable frequency fields we obtained $D_{\nu_c} = 0$ at $\nu_c = 2.5$ Hz, the curve of m_ν/m_{60} against ν being shown in figure 8. The measured $\nu_c = 2.5$ Hz is somewhat higher than the theoretical value (1.7 Hz) calculated from equation (49). Good agreement with the experimental findings was obtained when q was taken to be 0.55 instead of 0.46 as can be seen in figure 8, curve c_2; it can also be shown that a change in the parameter R does not produce significant change in the curves c_1 and c_2, at least in the present case. This

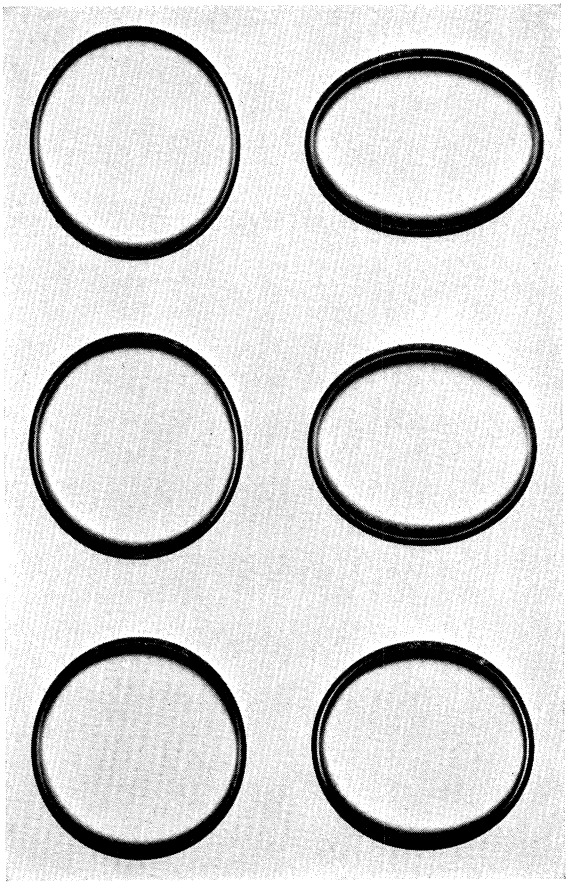

a.c. d.c.

FIGURE 7

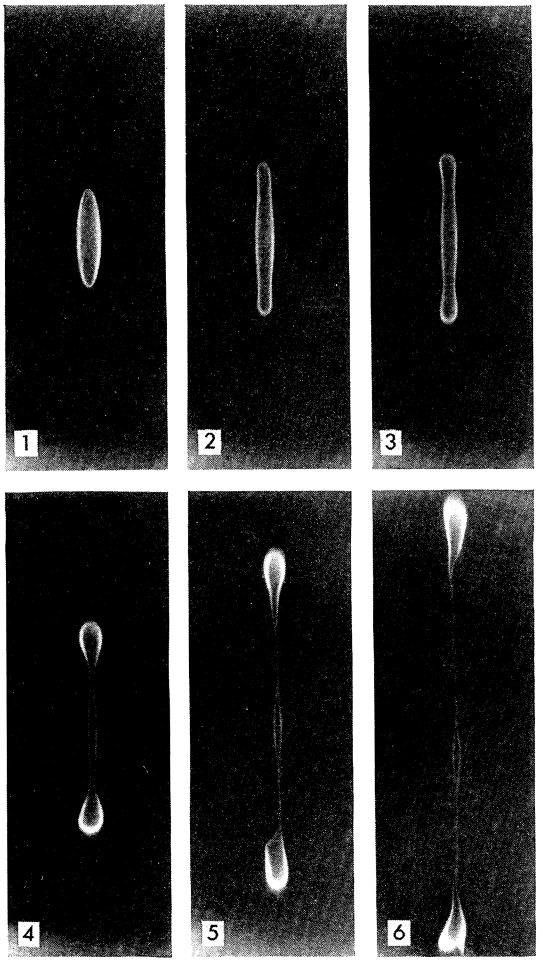

FIGURE 9

FIGURE 7. Photographs of electric deformation of a silicone oil drop suspended in castor oil (system 16). The drop is prolate in the a.c. electric field ($\nu = 60$ Hz) and oblate in the d.c. electric field ($\nu = 0$), the deformation increasing with the field $\bar{E}_0 = 1.5, 2.5, 3.5$ kV/cm from the bottom to the top; $b = 0.60$ mm.

FIGURE 9. Electric burst of system 7 at $\nu = 0$ with $b = 0.03$ cm; the time elapsed from frame 1 to 6 was about 0.1 s. The drop was split into two main parts connected by a thin thread which before breaking down rendered the system conductive by bridging the two electrodes. At burst $E_0 = 2.8$ kV/cm.

(*Facing p.* 314)

PHILOSOPHICAL TRANSACTIONS OF THE ROYAL SOCIETY A MATHEMATICAL, PHYSICAL & ENGINEERING SCIENCES

PHILOSOPHICAL TRANSACTIONS OF THE ROYAL SOCIETY A MATHEMATICAL, PHYSICAL & ENGINEERING SCIENCES

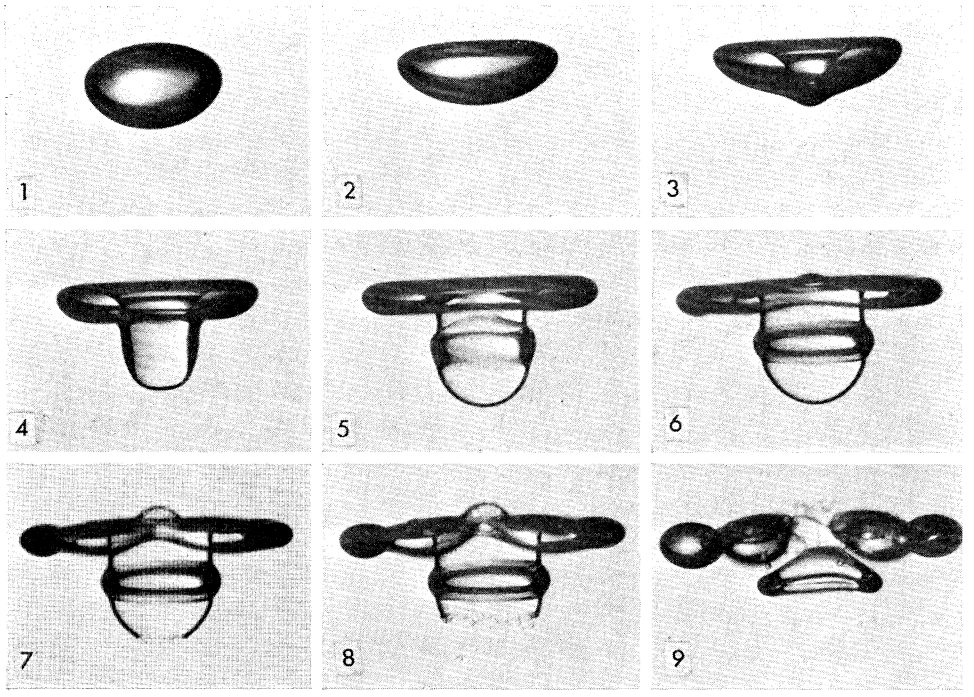

FIGURE 10

FIGURE 10. Mechanism of the electrohydrodynamic burst for system 16 at $\nu = 0$. The time elapsed from frame 1 to 9 was about 20 s, which was much longer than for the usual case of electric burst. The burst did not produce breakdown of the dielectric medium because the drop was much less conductive than the medium ($R > 30$), and it did not bridge the electrodes after bursting. The applied field $E_0 = 4.5\,\mathrm{kV/cm}$ and $b = 0.08\,\mathrm{cm}$.

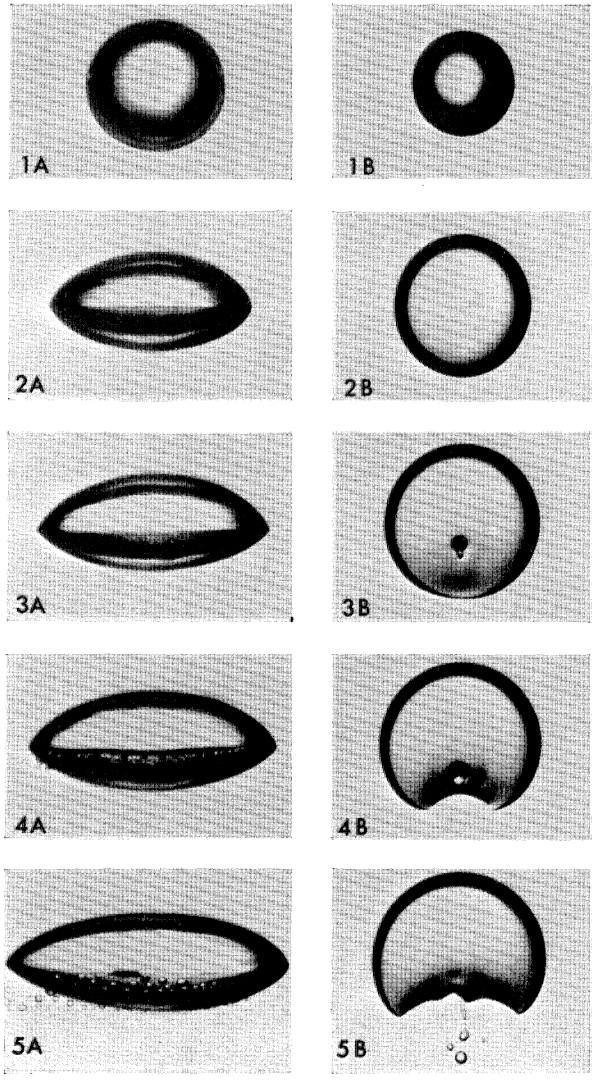

FIGURE 11

FIGURE 11. The photographs of the burst of two drops from system 16 at $\nu = 1\,\mathrm{Hz}$ showing the phenomena from two directions. In (A) the direction of $\boldsymbol{E}$ is vertical and in (B), photographed through the electrodes, normal to the sheet. The burst mechanism following the formation of a biconcave lens appears somewhat different in the two cases probably because of the difference of the drop radii and applied fields: (A) $b = 0.04\,\mathrm{cm}$ and $\overline{E}_0 = 4.5\,\mathrm{kV/cm}$; (B) $b = 0.06\,\mathrm{cm}$ and $\overline{E}_0 = 4.0\,\mathrm{kV/cm}$. The drop in frame 1B appears smaller than that in frame 1A because of smaller magnification.

suggests that accurate measurements of the dielectric constants of the phases are crucial to a quantitative test of equation (49).

The effect of the drop size on ν_c was also tested with system 18 over the range of b from 0.02 to 0.1 cm. No systematic variation of ν_c with b could be detected from which we concluded that ν_c was independent of b as predicted by equation (49).

4.2. *Fluid flow*

Several systems in class A_2 were examined for electrohydrodynamic flow in the phases but, as expected since $R \simeq 0$ and hence $F_{0\nu} \simeq 0$ (equation (20b)), none could be detected at $\nu = 0$, 60 Hz.

In system 3 of class A_1 ($Rq < 1$), the pattern of the flow field at $\nu = 0$ and at $\nu = 1$ Hz was as predicted by equations (23), i.e. equator-to-pole. Similarly, system 16 (class C, $Rq > 1$) was

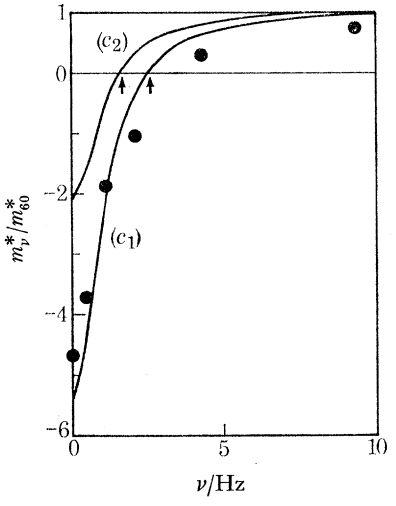

FIGURE 8. Illustrating the dependence of the ratio (m_ν^*/m_{60}^*) upon the field frequency ν for system 18 with $b = 0.64$ mm and $\bar{E}_0$ varying between 0.1 to 4 kV/cm. The points are the experimental values and the lines c_1 and c_2 were calculated from equations (48), (53) and (76) for the values of the electrical parameters in the following table. The arrows on the curves indicate ν_c calculated from equation (49).

	R	q	a	ν_c/Hz
c_1	21	0.55	2.5	2.5
c_2	21	0.46	2.5	1.6

pole-to-equator both at $\nu = 0$ and $\nu = 1$ Hz; this confirms the observations reported by Taylor (1966) at $\nu = 0$. As ν was increased beyond 1 Hz, the flow rate diminished rapidly as would be expected from equation (36b). Thus, qualitatively, the theory of electrohydrodynamic flow in both steady and alternating fields was confirmed.

4.3. *Oscillatory deformation*

It is readily shown from equation (66) that $D_T \ll D_\nu$ for all the systems used when $b \geqslant 0.02$ cm. However, at $\nu = 1$ Hz, the smallest attainable, with system 21, which had a small k, the drop could be seen to oscillate twice as fast as the field. Small oscillations of the drop surface were also observed for systems 11 and 16 at $\nu = 1$ Hz when very high fields were applied, the drop being close to burst. This is in accordance with equation (62). As ν increased the amplitude of the oscillations became smaller as predicted by equation (66) since k increased.

4.4. *Drop burst*

At high electric fields two distinct modes of burst were observed by Allan & Mason (1962) in their experiments at $\nu = 0$, one when $D_0 > 0$ and the other when $D_0 < 0$. An approximate theory based on the idea that burst occurs when the normal electric stress can no longer be contained by the interfacial tension served to explain the first mode of burst (Allan & Mason 1962); in the light of the theory we have presented we can call this 'electric burst' since it characterizes systems in which $F'_{\theta\nu} = 0$ (class A_2) and there is no electro-hydrodynamic flow inside and outside the drop. We have found that the second mode, in which an oblate spheroid burst by being squashed occurred in systems of class C at zero or low frequencies where the hydrodynamic stress contributed to burst; we define this as 'electrohydrodynamic burst'. The classification of the systems given in equations (54) and illustrated in figure 2 suggests that electrohydrodynamic burst should also characterize all the systems for which $D_\nu \neq 0$ and $F'_{\theta\nu} \neq 0$ (i.e. $R \neq 0$ and $Rq \neq 1$) even when $f_{r\nu}$ produces a prolate deformed drop. This suggests that the electrohydrodynamic burst should show different mechanisms depending upon the contribution of the shear stress which depends upon the frequency of the applied field (equation (35)), upon the electrical properties of the systems (equations (54)) and upon the drop radius since at burst the deformation is large.

Electric burst is illustrated by the cinematographs in figure 9, plate 6, taken in system 7 at $\nu = 0$; similar behaviour was found at $\nu = 60$ Hz. When the electric field was increased very slowly up to the value at burst (a rapid increase of $\bar{E}_0$ may produce different modes of burst since the drop cannot rearrange its shape to balance the increasing electric stress), the drop elongated until it formed a rod with rounded ends which then split into two main parts joined by a thread which subsequently broke into a number of small drops.

Two modes of electrodynamic burst are illustrated by the cinematographs in figures 10 and 11, plate 7, with system 16 at $\nu = 0$, $\nu = 1$ Hz respectively; for this system the calculated $\nu_c = 8$ Hz.

Figure 10, plate 7, shows that at $\nu = 0$ the drop flattened into an oblate spheroid (frame 1) and lost its symmetrical shape because of the migration towards the positive electrode as already observed (frame 2); after a further increase in E_0, a jet of the suspending medium penetrated into the migrating drop of the rear (frame 3) generating a column of phase 2 surrounded by a thin film of phase 1 (frame 4). The column enlarged while the phase 1 film drained (frames 5, 6) until it collapsed (frames 7, 8) generating five big droplets and a myriad of tiny ones (frame 9).

Figure 11 shows that at $\nu = 1$ Hz the mechanism was somewhat different probably because of the absence of migration and of the decreased effect of the shear stress (equation (35)), the drop becoming flattened into a biconcave lens with the sharp edge normal to the electric field from which tiny drops were expelled. The phenomenon is illustrated by photographs taken in different directions with respect to the field.

Other more complicated types of electrohydrodynamic burst were observed in other systems; for example in system 22 at $\nu = 0$ the drop flattened and then folded over and twisted until it was no longer coplanar, the manner of burst probably being influenced by the simultaneous electrophoretic migration occurring at $\nu = 0$. Further experimentation is needed before the various modes of burst can be characterized in detail and a complete theory proposed.

5. Concluding remarks

We wish to emphasize that the theory was developed after performing the experiments, and for this reason a complete experimental test of it is not available from the data. The theory does, however, explain most of the observations: deformation classes A_1, A_2 and C, the existence of ν_c in class C and the reversal in electrohydrodynamic streaming at $Rq = 1$.

Experiments were not made with systems belonging to class B, nor falling on line (AB) or (BC) of figure 2, nor falling in class C with $\nu_c > 60$ Hz or $q = 1$ for which $\nu_c = \infty$. Frequencies high enough (> 60 Hz) were not used to establish if $(\partial D_\nu/\partial\nu) < 0$ in systems of class A_2 as predicted by equation (71). It would be interesting to include such experiments in future work.

The most serious discrepancy was that in nearly all cases $(m_\nu^*/m_\nu) > 1$, indicating larger deformations than predicted. This is similar to the findings of Allan & Mason (1962) at $\nu = 0$ who suggested, without proof, that the discrepancy may have been an electrocapillarity effect by which the apparent γ was lowered by the accumulation of a net electric charge at the interface.

Effects which we wish to examine further are surface conductance and convection of charge neglected in the theory. Considering surface conductance first, we note from equation (73) that its contribution to $\nabla_2 Q_S$ is

$$\nabla_2 \frac{E_{2\theta}}{\chi_{12}} = -6E_0 \frac{\mathrm{Re}\,(A\,\mathrm{e}^{\mathrm{i}\omega t})}{b\chi_{12}} \cos\theta, \tag{78}$$

which when substituted into equation (75) yields

$$\frac{b\chi_{12}}{\chi_1} \gg 2 \quad \text{or} \quad \frac{b\chi_{12}}{\chi_1} \gg \frac{2}{R}\sqrt{\left(\frac{R^2+a^2\omega^2}{1+a^2\omega^2q^2}\right)}, \tag{79}$$

as conditions to be satisfied for the theory to apply. We do not know the values of χ_{12} for our systems, but it is evident from equations (78) and (74d) that a finite χ_{12} will produce an increase of the algebraic value of the charges facing the negative electrode and a decrease of those facing the positive electrode, hence producing an increase in the algebraic value of D_ν (the effect is analogous to that of increasing the conductivity of the drop) which will be still linear in $\bar{E}_0^2$ but not in $(\bar{E}_0^2 b)$ because the term $(\chi_{12} b)$ contains b.

Our results did not show a systematic deviation from linearity when D_ν was plotted against $(\bar{E}_0^2 b)$ when both $\bar{E}_0$ and b were varied. A small χ_{12} might explain $(m_\nu^*/m_\nu) > 1$ for systems of class A_1 and class A_2 both at $\nu = 0$ and at $\nu = 60$ Hz. However, for class C it should have yielded $(m_0^*/m_0) < 1$ instead of $(m_0^*/m_0) > 1$. The evidence for this effect is therefore inconclusive.

The contribution to $\nabla_2 Q_S$ from convection of charge, equivalent to a streaming current, is from equation (73)

$$\nabla_2(\sigma u_{2\theta}) = \frac{27\epsilon_0^2 K_2^2 E_0^3}{5(\mu_1+\mu_2)} S(2\cos^2\theta - 1)\cos\theta, \tag{80}$$

where

$$S = \frac{(1-Rq)\,(S_1+S_2)}{\sqrt{\{(2R+1)^2 + a^2\omega^2(q+2)^2\}}} \cos(\omega t - \alpha_\nu) \tag{81a}$$

and

$$S_1 = \frac{(3\lambda+2)kI}{4\sqrt{(1+k^2\lambda_2^2)}} \sin(2\omega t + \alpha_\nu^{\mathrm{II}}), \tag{81b}$$

$$S_2 = \frac{(Rq-1)\,[R + \sqrt{(R^2+a^2\omega^2)}\cos(2\omega t + \alpha_\nu^{\mathrm{I}})]}{(2R+1)^2 + a^2\omega^2(q+2)^2}. \tag{81c}$$

Substituting equation (80) into equations (75) we obtain as a condition for validity of the theory

$$\bar{E}_0 \ll (\bar{E}_0)_{\max} \tag{82}$$

$$(\bar{E}_0)_{\max} = \frac{1}{3\epsilon_0 K_2}\sqrt{\frac{\mu_2}{\chi_1}}\sqrt{g_{\min}} \tag{83}$$

and $g_{\min}$ is the smallest of the following four functions:

$$g_1 = 5(1+\lambda)\frac{(2R+1)^2+a^2\omega^2(q+2)^2}{2(1-Rq)^2}, \tag{84a}$$

$$g_2 = g_1 R\sqrt{\frac{1+a^2\omega^2q^2}{R^2+a^2\omega^2}}, \tag{84b}$$

$$g_3 = \frac{10(1+\lambda)\sqrt{(R^2+a^2\omega^2)}}{k(3\lambda+2)I|1-Rq|}\sqrt{(1+k^2\lambda_2^2)}, \tag{84c}$$

$$g_4 = g_3 R\sqrt{\frac{1+a^2\omega^2q^2}{R^2+a^2\omega^2}}. \tag{84d}$$

Equation (83), unlike equation (79), imposes a restriction on the upper limit of the field strength to which the theory is applicable. Our experimental conditions, in which $\bar{E}_0$ was varied from 0.01 to 5 kV/cm, satisfied equation (82) in most of the systems as shown in table 2 where $(\bar{E}_0)_{\max}$ calculated from equation (83), is given. Furthermore, inspection of equations (80) and (74*d*) shows that the effect on $\partial\sigma/\partial t$ of the convection of charge is proportional to $E_0^2(2\cos^2\theta-1)$, which leads to the result that (i) the drop is no longer ellipsoidal and (ii) D_v is not linear in $\bar{E}_0^2 b$, neither mode of behaviour having been observed. We can thus conclude that the convection of charge at the interface did not play an important role in our experiments.

Other possible reasons for the discrepancy are: (i) limitations in the electric model assumed in the theory which is described by the boundary conditions listed after equation (2), (ii) effects of space charges which were taken to be zero in equation (2), and (iii) effects due to diffuse ionic layers at the interface. These, together with the inclusion of the inertial terms in the Navier–Stokes equations at high ν, are aspects which ought to be examined in any further theoretical and experimental studies.

Finally we mention two interesting possibilities which are suggested by the theory. In figure 1*b* it is shown that the polarization of the drop is reversed when going from $Rq > 1$ to $Rq < 1$, suggesting that a pair of such drops will repel one another; in a study of the interaction of pairs of immiscible drops in a third liquid (Torza & Mason 1970) we observed repulsion in several systems in which one drop had $Rq > 1$ and the other $Rq < 1$. In two phase emulsions of class C, the application of a field of frequency ν_e may be expected to cause electric breaking with unlimited growth in drop size since no electric deformation and hence burst would occur as the drops increase in size; otherwise there would be an upper limit to the b attained by coalescence at a given field strength.

This work was assisted by the Defence Research Board of Canada (DRB grant no. 9530–47).

References

Allan, R. S. & Mason, S. G. 1962 *Proc. Roy. Soc. Lond.* A**267**, 45.
Buchner, E. H. & Van Royen, A. H. H. 1929 *Kolloid Z.* **49**, 249.
Garton, C. G. & Krasucki, Z. 1964 *Proc. Roy. Soc. Lond.* A**280**, 211.
Goldstein, S. (ed.) 1938 *Modern developments in fluid dynamics*. Oxford University Press.
Harnwell, G. P. 1949 *Principles of electricity and electromagnetism*. (2nd ed.), p. 650. New York: MacGraw-Hill.
Iribarne, J. V. & Mason, B. J. 1967 *Trans. Faraday Soc.* **53**, 2235.
Jeans, Sir James 1960 *Mathematical theory of electricity and magnetism* (5th ed.), p. 153. Cambridge University Press.
Kao, K. C. 1961 *Br. J. app. Phys.* **12**, 628.

PHILOSOPHICAL TRANSACTIONS OF THE ROYAL SOCIETY A MATHEMATICAL, PHYSICAL & ENGINEERING SCIENCES

Melcher J. R. & Taylor, G. I. 1969 *Annual Rev. Fluid Mech.* **1**, 127.
Nayyar, N. K. & Murthy, G. S. 1959 *Proc. natn. Inst. Sci. India* A **25**, 373.
O'Konski, C. T. & Thacher, H. C. 1953 *J. phys. Chem.* **57**, 995.
O'Konski, C. T. & Gunther, R. L. 1955 *J. Colloid Sci.* **10**, 563.
O'Konski, C. T. & Harris, F. E. 1957 *J. phys. Chem.* **61**, 1172.
Rumscheidt, F. D. & Mason, S. G. 1961 *J. Colloid Sci.* **16**, 238.
Schwarz, G. 1962 *J. phys. Chem.* **66**, 2636.
Smythe, W. R. 1959 *Static and dynamic electricity* (2nd ed.). New York: McGraw-Hill.
Taylor, Sir Geoffrey 1964 *Proc. Roy. Soc. Lond.* A **280**, 383.
Taylor, Sir Geoffrey 1966 *Proc. Roy. Soc. Lond.* A **291**, 159.
Torza, S. & Mason, S. G. 1970 *J. Colloid Interface Sci.* **33**, 68.
Wilson, C T. R. & Taylor, G. I. 1925 *Proc. Camb. Phil. Soc.* **22**, 728.

PHILOSOPHICAL TRANSACTIONS OF THE ROYAL SOCIETY A MATHEMATICAL, PHYSICAL & ENGINEERING SCIENCES

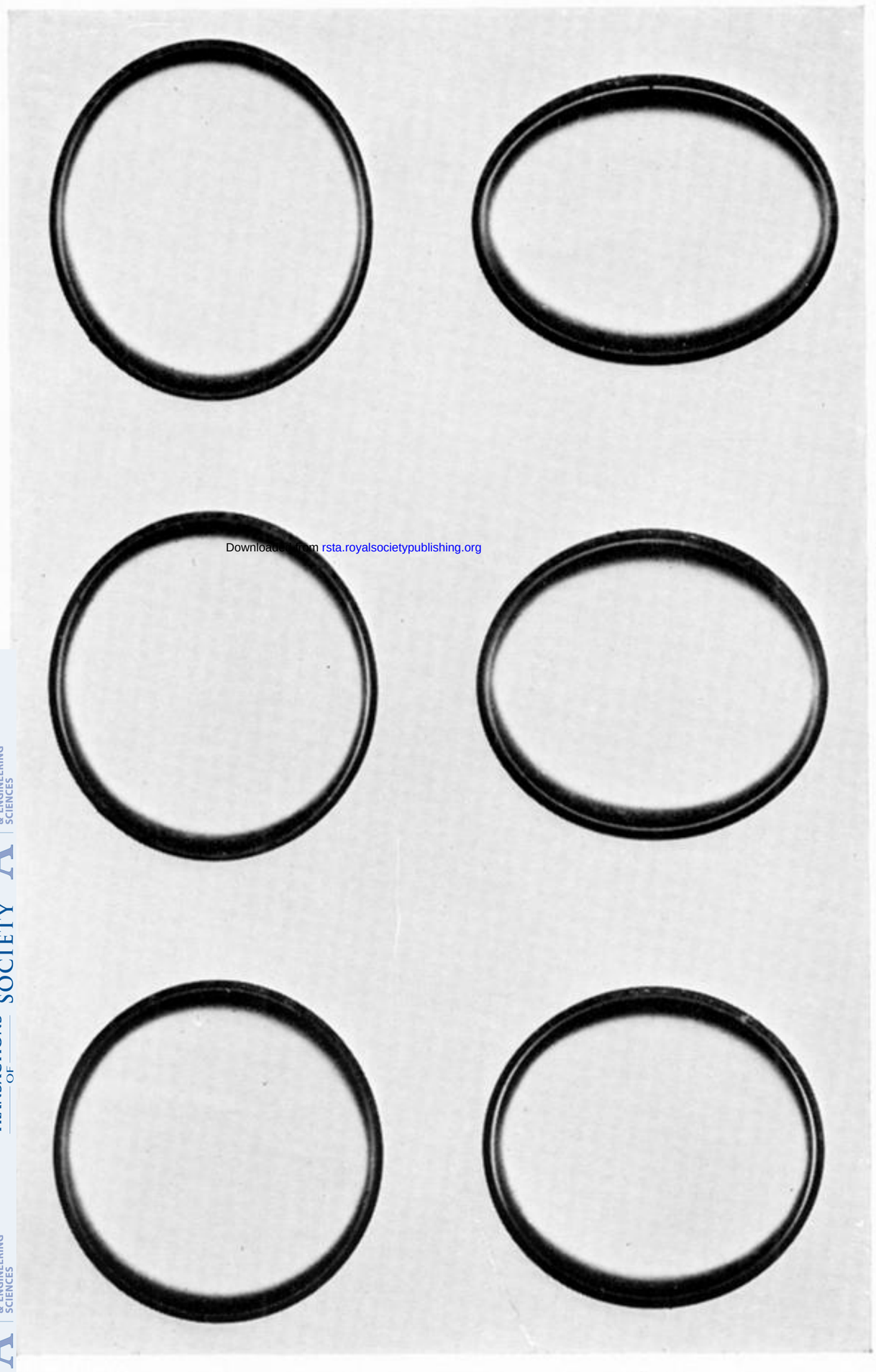

a.c. d.c.

FIGURE 7

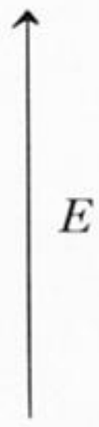

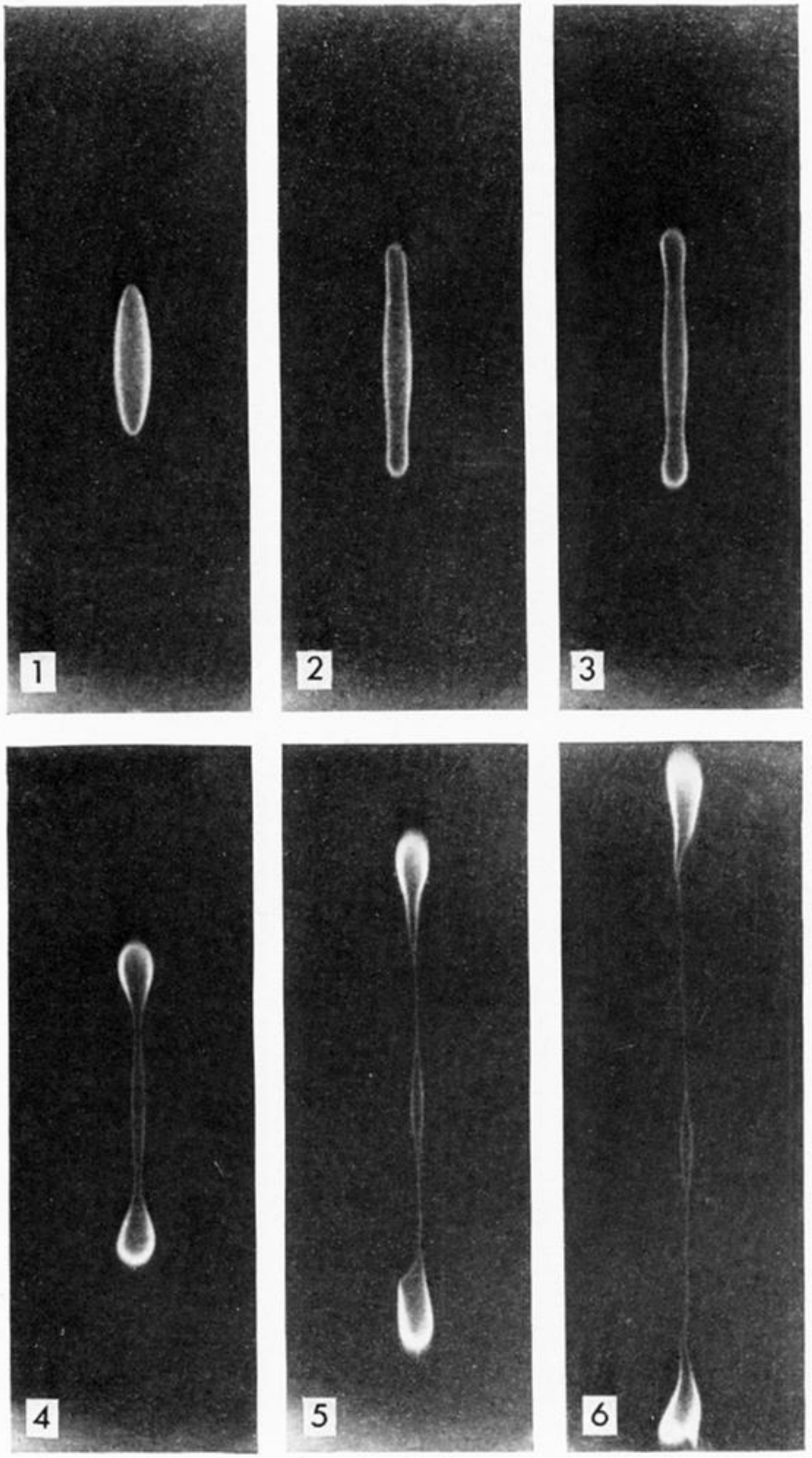

FIGURE 9

FIGURE 7. Photographs of electric deformation of a silicone oil drop suspended in castor oil (system 16). The drop is prolate in the a.c. electric field ($\nu = 60\,\mathrm{Hz}$) and oblate in the d.c. electric field ($\nu = 0$), the deformation increasing with the field $\overline{E}_0 = 1.5, 2.5, 3.5\,\mathrm{kV/cm}$ from the bottom to the top; $b = 0.60\,\mathrm{mm}$.

FIGURE 9. Electric burst of system 7 at $\nu = 0$ with $b = 0.03$ cm; the time elapsed from frame 1 to 6 was about 0.1 s. The drop was split into two main parts connected by a thin thread which before breaking down rendered the system conductive by bridging the two electrodes. At burst $E_0 = 2.8\,\mathrm{kV/cm}$.

PHILOSOPHICAL TRANSACTIONS OF THE ROYAL SOCIETY A MATHEMATICAL, PHYSICAL & ENGINEERING SCIENCES

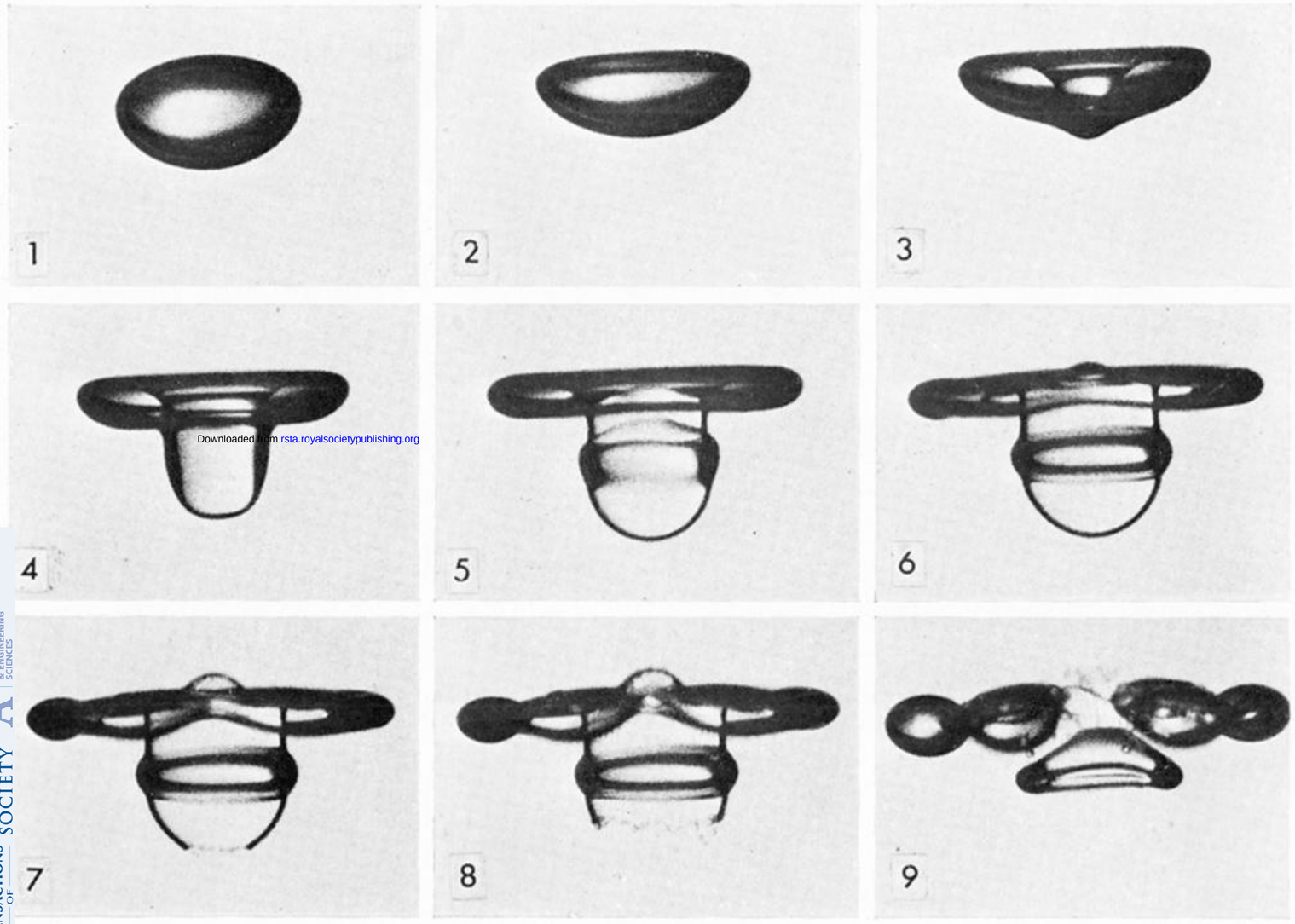

FIGURE 10

FIGURE 10. Mechanism of the electrohydrodynamic burst for system 16 at $\nu = 0$. The time elapsed from frame 1 to 9 was about 20 s, which was much longer than for the usual case of electric burst. The burst did not produce breakdown of the dielectric medium because the drop was much less conductive than the medium ($R > 30$), and it did not bridge the electrodes after bursting. The applied field $E_0 = 4.5\,\mathrm{kV/cm}$ and $b = 0.08\,\mathrm{cm}$.

FIGURE 11. The photographs of the burst of two drops from system 16 at $\nu = 1\,\mathrm{Hz}$ showing the phenomena from two directions. In (A) the direction of $\boldsymbol{E}$ is vertical and in (B), photographed through the electrodes, normal to the sheet. The burst mechanism following the formation of a biconcave lens appears somewhat different in the two cases probably because of the difference of the drop radii and applied fields: (A) $b = 0.04\,\mathrm{cm}$ and $\overline{E}_0 = 4.5\,\mathrm{kV/cm}$; (B) $b = 0.06\,\mathrm{cm}$ and $\overline{E}_0 = 4.0\,\mathrm{kV/cm}$. The drop in frame 1B appears smaller than that in frame 1A because of smaller magnification.

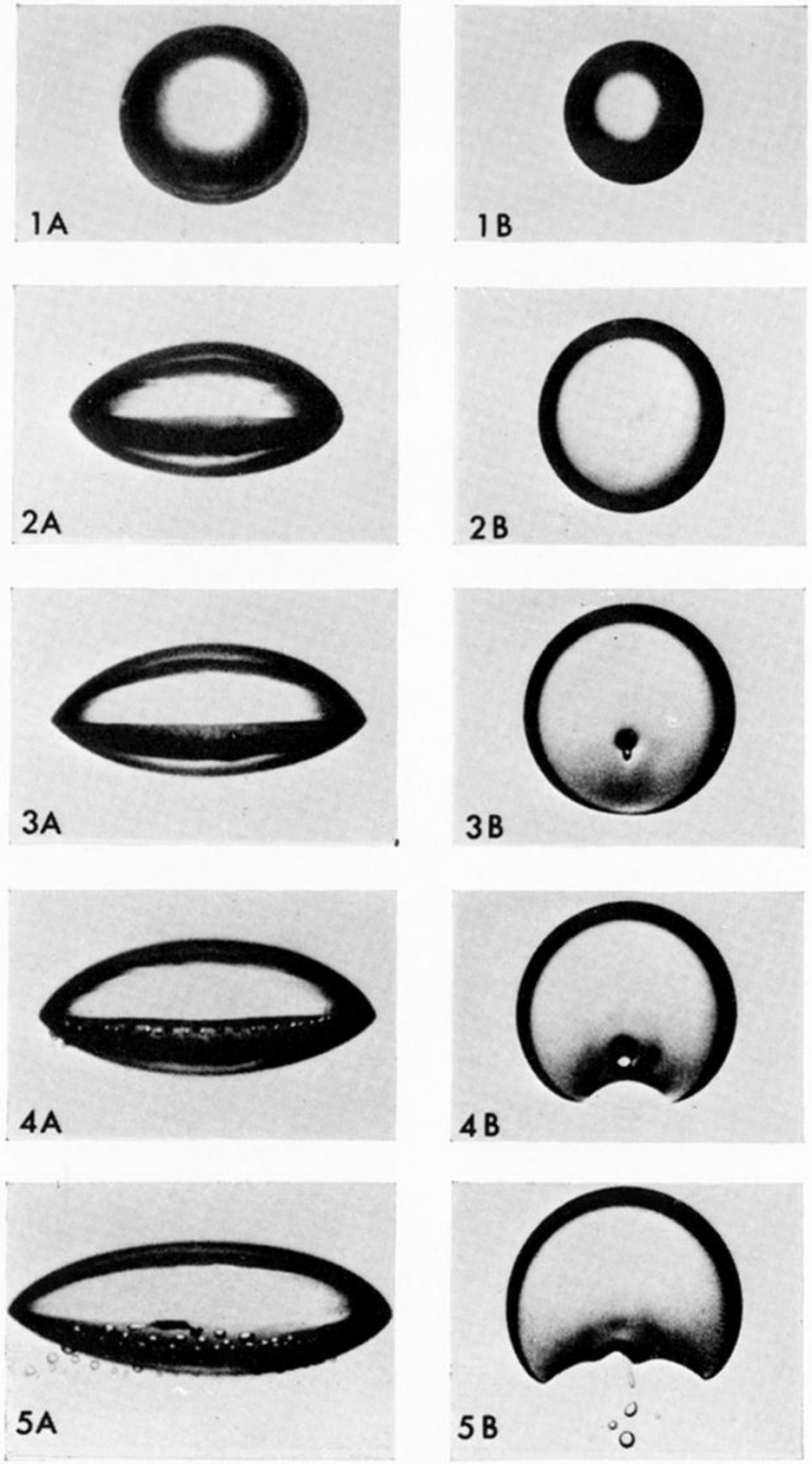

FIGURE 11